



**HAL**  
open science

# Controls on Cenozoic exhumation of the Tethyan Himalaya from fission-track thermochronology and detrital zircon U-Pb geochronology in the Gyirong basin area, southern Tibet

Tianyi Shen, Guocan Wang, Philippe Hervé Leloup, Peter van Der Beek, Matthias Bernet, Kai Cao, An Wang, Chao Liu, Kexin Zhang

## ► To cite this version:

Tianyi Shen, Guocan Wang, Philippe Hervé Leloup, Peter van Der Beek, Matthias Bernet, et al.. Controls on Cenozoic exhumation of the Tethyan Himalaya from fission-track thermochronology and detrital zircon U-Pb geochronology in the Gyirong basin area, southern Tibet. *Tectonics*, 2016, 35 (7), pp.1713-1734. 10.1002/2016TC004149 . hal-02331993

**HAL Id: hal-02331993**

**<https://univ-lyon1.hal.science/hal-02331993>**

Submitted on 21 Sep 2021

**HAL** is a multi-disciplinary open access archive for the deposit and dissemination of scientific research documents, whether they are published or not. The documents may come from teaching and research institutions in France or abroad, or from public or private research centers.

L'archive ouverte pluridisciplinaire **HAL**, est destinée au dépôt et à la diffusion de documents scientifiques de niveau recherche, publiés ou non, émanant des établissements d'enseignement et de recherche français ou étrangers, des laboratoires publics ou privés.

Copyright



## Tectonics

### RESEARCH ARTICLE

10.1002/2016TC004149

#### Key Points:

- Sedimentation in the Gyirong basin is controlled by the N-S Gyirong normal fault, not by the STDS
- Widespread ~15–18 Ma exhumation event in southern Tibet and the Himalaya
- Exhumation slowed down in southern Tibet since ~16 Ma, while rapid exhumation continued in the Greater Himalaya

#### Supporting Information:

- Supporting Information S1
- Table S1

#### Correspondence to:

G. Wang,  
wgcan@cgug.edu.cn

#### Citation:

Shen, T., G. Wang, P. H. Leloup, P. van der Beek, M. Bernet, K. Cao, A. Wang, C. Liu, and K. Zhang (2016), Controls on Cenozoic exhumation of the Tethyan Himalaya from fission-track thermochronology and detrital zircon U-Pb geochronology in the Gyirong basin area, southern Tibet, *Tectonics*, 35, 1713–1734, doi:10.1002/2016TC004149.

Received 3 FEB 2016

Accepted 27 JUN 2016

Accepted article online 4 JUL 2016

Published online 19 JULY 2016

©2016. American Geophysical Union.  
All Rights Reserved.

## Controls on Cenozoic exhumation of the Tethyan Himalaya from fission-track thermochronology and detrital zircon U-Pb geochronology in the Gyirong basin area, southern Tibet

Tianyi Shen<sup>1,2</sup>, Guocan Wang<sup>1,2</sup>, Philippe Hervé Leloup<sup>3</sup>, Peter van der Beek<sup>4</sup>, Matthias Bernet<sup>4</sup>, Kai Cao<sup>1,2</sup>, An Wang<sup>1,2</sup>, Chao Liu<sup>5</sup>, and Kexin Zhang<sup>6</sup>

<sup>1</sup>Center for Global Tectonics, School of Earth Sciences, China University of Geosciences, Wuhan, China, <sup>2</sup>State Key Laboratory of Geological Processes and Mineral Resources, China University of Geosciences, Wuhan, China, <sup>3</sup>Laboratoire des Sciences de la Terre de Lyon, Terre, Planètes, Environnement, Université de Lyon, UMR CNRS 5276, Lyon, France, <sup>4</sup>Institut des Sciences de la Terre, Université Grenoble Alpes, Grenoble, France, <sup>5</sup>Department of Land and Resources of Liaoning Province, Shenyang, China, <sup>6</sup>State Key Laboratory of Biogeology and Environmental Geology, China University of Geosciences, Wuhan, China

**Abstract** The Gyirong basin, southern Tibet, contains the record of Miocene-Pliocene exhumation, drainage development, and sedimentation along the northern flank of the Himalaya. The tectonic controls on basin formation and their potential link to the South Tibetan Detachment System (STDS) are not well understood. We use detrital zircon (ZFT) and apatite (AFT) fission-track analysis, together with detrital zircon U-Pb dating to decipher the provenance of Gyirong basin sediments and the exhumation history of the source areas. Results are presented for nine detrital samples of Gyirong basin sediments (AFT, ZFT, and U-Pb), two modern river-sediment samples (ZFT and AFT), and six bedrock samples (ZFT) from transect across the Gyirong fault bounding the basin to the east. The combination of detrital zircon U-Pb and fission-track data demonstrates that the Gyirong basin sediments were sourced locally from the Tethyan Sedimentary Sequence. This provenance pattern indicates that deposition was controlled by the Gyirong fault, active since ~10 Ma, whose vertical throw was probably < ~5000 m, rather than being controlled by normal faults associated with the STDS. The detrital thermochronology data contain two prominent age groups at ~37–41 and 15–18 Ma, suggesting rapid exhumation at these times. A 15–18 Ma phase of rapid exhumation has been recorded widely in both southern Tibet and the Himalaya. A possible interpretation for such a major regional exhumation event might be detachment of the subducting Indian plate slab during the middle Miocene, inducing dynamic uplift of the Indian plate overriding its own slab.

### 1. Introduction

The Himalayan range is the largest continental collisional mountain belt on Earth and forms the southern boundary of the world's largest orogenic plateau: the Tibetan Plateau. The cooling history of rocks within the mountain range and the sedimentation history of the adjacent basins provide invaluable constraints on the orogenic exhumation history and mechanisms, required for a better understanding of the evolution of the Himalayan orogen and the Tibetan Plateau [e.g., Najman, 2006; Yin, 2006]. A large number of thermochronologic studies have been conducted across the Himalaya (for a review, see Thiede and Ehlers [2013]) and southern Tibet [e.g., Copeland et al., 1995; Dai et al., 2013; Carrapa et al., 2014; Li et al., 2015]. Similarly, the sedimentation history in the foreland basins to the south [e.g., DeCelles et al., 1998; Najman and Garzanti, 2000; Mugnier and Huyghe, 2006] and north [e.g., DeCelles et al., 2011, 2014] of the Himalayan orogen has received significant attention in recent years. However, bedrock thermochronology studies have focused mainly on the Greater Himalayan Sequence (GHS) and the southern flank of the mountain belt [cf. Thiede and Ehlers, 2013], whereas relatively little is known about the exhumation history of the Tethyan Sedimentary Sequence (TSS) on the northern flank.

Since the onset of India-Asia collision, the TSS has been affected by ~N-S shortening [e.g., Murphy and Yin, 2003] and at least two phases of Neogene syn-orogenic extension, with the development of the South Tibetan Detachment System (STDS) [e.g., Burg et al., 1984; Burchfiel et al., 1992] and north-south trending normal faults [e.g., Armijo et al., 1986]. The STDS is a large-scale west-east trending fault system that stretches for

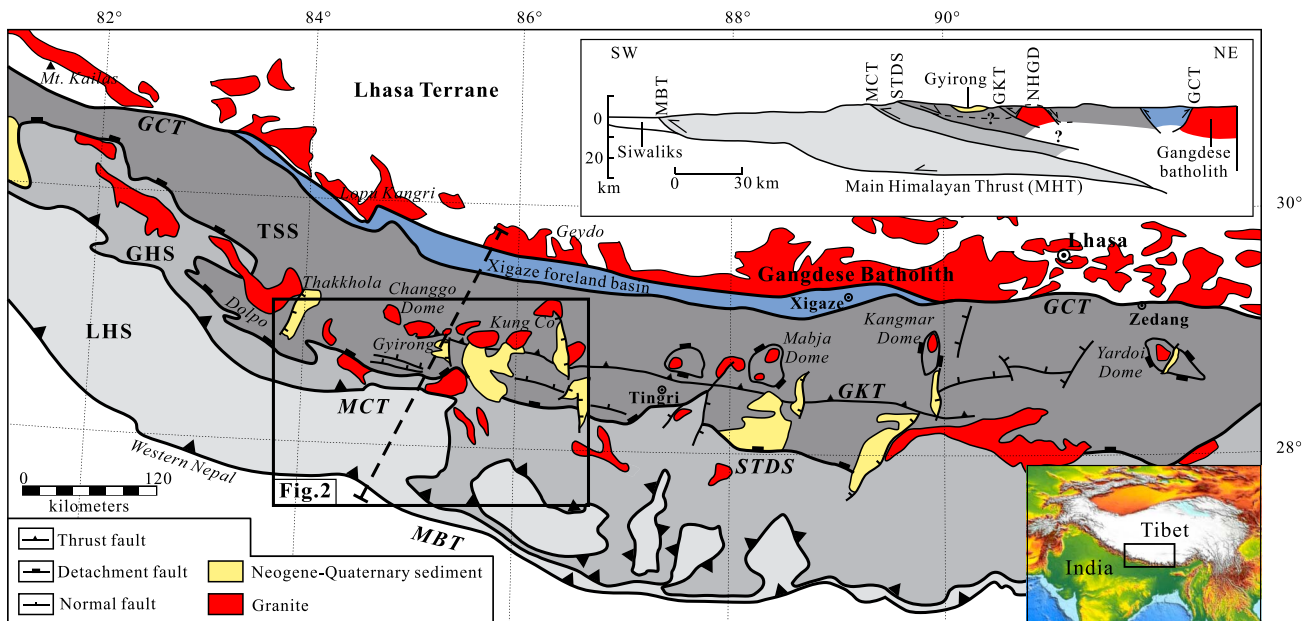


**Figure 1.** Simplified structural map and cross section (top inset) of Southern Tibet and the central Himalaya, after *Burchfiel et al.* [1992], *Lee et al.* [2000], *Larson et al.* [2010], *Kali et al.* [2010], *Wang et al.* [2011, 2014], and *Leloup et al.* [2015]. The box outlines the location of Figure 2, and the dashed line indicates the position of cross section. Abbreviations: MBT, Main Boundary Thrust; MCT, Main Central Thrust; STDS, South Tibetan Detachment System; GKT, Gyrong-Kangmar Thrust; TSS, Tethyan Sedimentary Sequence; GHS, Greater Himalayan Sequence; LHS, Lesser Himalayan Sequence; and NHGD, North Himalayan Gneiss domes. Black box (bottom inset) shows the position of the main map in Asia.

more than 1000 km in the hinterland of the Himalayan orogen (Figure 1). It comprises a shallowly dipping ductile shear zone (sometimes referred to as the lower STDS) and a network of brittle-ductile faults (sometimes referred to as the upper STDS) that locally partly excise and overprint the earlier mylonite. Some consider that the two sets of structures correspond to a single south dipping normal fault zone that evolved from ductile to brittle [e.g., *Law et al.*, 2004; *Leloup et al.*, 2010, 2015]. Other authors argue that the shear zone is not a normal fault but the upper limit of south directed flow in a horizontal crustal channel, later locally exhumed by the low-angle brittle-ductile normal faults [e.g., *Kellett and Grujic*, 2012]. The north-south trending faults are steeply dipping normal faults. Given their different dips, these two different types of faults could have induced two different types of basins, known as supradetachment basins and rift basins, respectively [*Friedmann and Burbank*, 1995].

Neogene-Quaternary intermontane basins have been described throughout southern Tibet (Figure 1). Some basins, particularly the Gyrong basin located just north of the topographic culmination of the Himalaya, have been interpreted as related to low-angle normal fault movement on the upper STDS [*Burchfiel et al.*, 1992; *Hodges*, 2000], whereas north-south elongated rift basins, such as the Thakkhola graben [e.g., *Colchen*, 1999; *Garzione et al.*, 2003], are associated with the north-south trending normal faults (Figure 1). However, the few Neogene basins that have been described as related to the STDS are all located in or immediately next to major Neogene north-south trending rifts. In the central Himalaya, movement along the STDS continued until 13–11 Ma [*Kali et al.*, 2010; *Leloup et al.*, 2010; *Wang et al.*, 2010]. N-S trending normal faults in southern Tibet may have initiated prior to 11 Ma but appear to have accelerated after 10 Ma [*Sundell et al.*, 2013]. Thus, while the N-S normal faults clearly cut and offset the STDS where they intersect, such as in Dinggye [*Kali et al.*, 2010] and Yadong [*Armijo et al.*, 1986; *Cogan et al.*, 1998; *Wu et al.*, 1998; *Ratschbacher et al.*, 2011; *Kellett and Grujic*, 2012; *Kellett et al.*, 2013], the activity of both fault systems may have overlapped for a few million years, making it difficult to differentiate whether basin development was related to movement on the STDS or to younger east-west extension [*Yin*, 2006].

In order to address these problems, we present a combined detrital zircon U-Pb geochronology and fission-track thermochronology study of the Neogene sedimentary rocks of the Gyrong basin, located ~20 km north of the lower STDS in southern Tibet (Figures 1–3). Several authors [*Burchfiel et al.*, 1992; *Hodges*, 2000; *Yang et al.*, 2009]

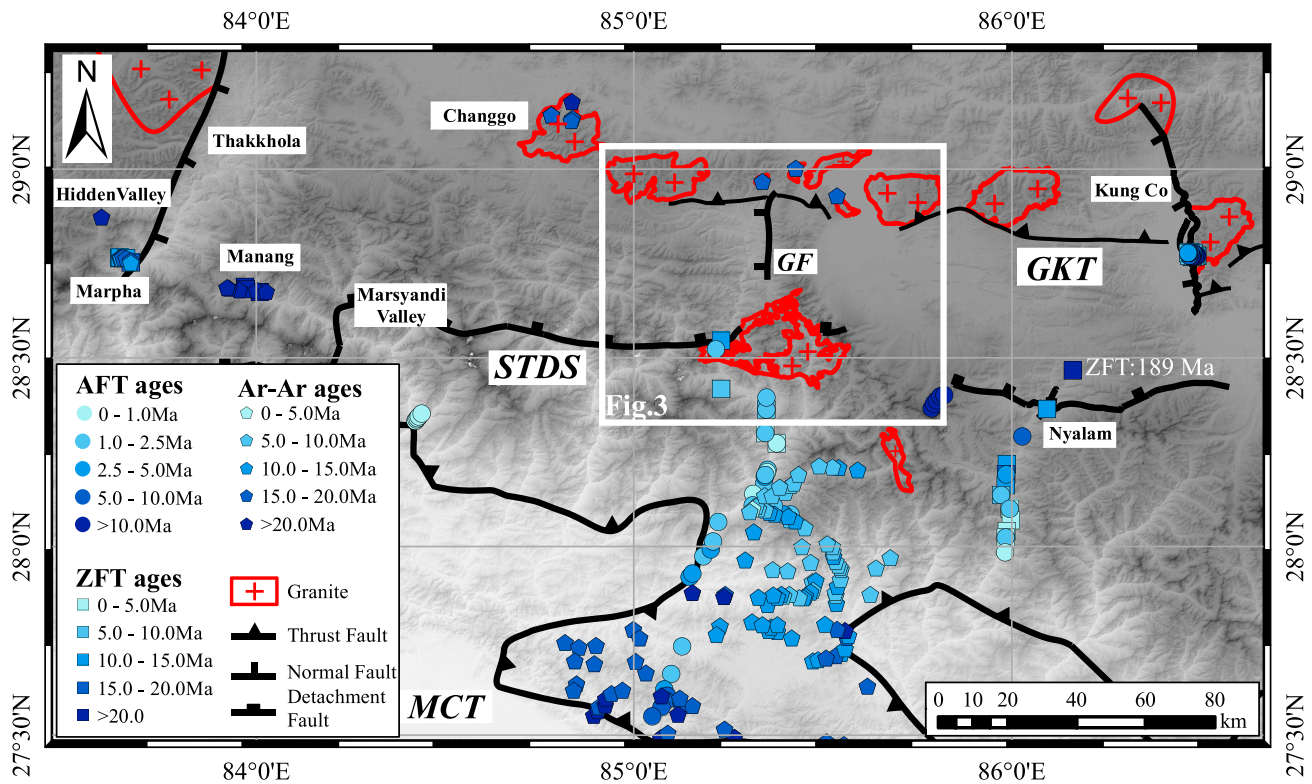


**Figure 2.** Shaded-relief map of the central Himalaya showing the main tectonic features and available thermochronology data. GF, Gyirong Fault; STDS, South Tibetan Detachment System; MCT, Main Central Thrust; and GKT, Gyirong-Kangmar Thrust. Shaded-relief map was produced by ArcGis and is based on the Advanced Spaceborne Thermal Emission and Reflection Global Digital Elevation Model. Thermochronology data are from Searle et al. [1997], Aoya et al. [2005, 2006], Huntington et al. [2006], Crouzet et al. [2007], Kawakami et al. [2007], Robert et al. [2009], Wang et al. [2010], Herman et al. [2010], and Li et al. [2013].

have inferred that low-angle north dipping, E-W trending normal faults associated with the STDS are genetically related to the formation of this basin, the northernmost of these faults forming the southern boundary of the Neogene clastic sequence and placing these rocks onto TSS rocks (inset of Figure 3). Burchfiel et al. [1992] interpreted this boundary as the primary fault controlling the development of the Gyirong basin. However, the N-S trending and west-dipping Gyirong Fault (GF), which forms the eastern boundary of the basin, appears much more prominent on remote sensing imagery than the north dipping E-W trending fault and controls the present-day topography of this area (Figure 2). Limited studies within the Gyirong basin [Wang et al., 1996; Yue et al., 2004; Yang et al., 2009; Xu et al., 2012] have not been conclusive as to whether the low-angle normal faults associated with the STDS or the GF control deposition in the basin.

The aims of our study are to constrain the provenance of the Gyirong basin fill, as well as the exhumation and sedimentation history of the area. In order to do so, we present new bedrock and detrital (apatite and zircon fission-track) thermochronology data combined with detrital zircon U-Pb geochronology. These data allow a better understanding of the controls on the development of the basin, as well as on the history and mechanisms of exhumation of the Tethyan Himalaya in southern Tibet.

## 2. Geological Setting

### 2.1. Regional Tectonics

The Himalaya lies between the Indian craton to the south and the Indus-Yarlung suture zone to the north (Figure 1). It is subdivided into three main tectonic units: the Lesser Himalayan Sequence (LHS), GHS, and TSS, bounded by three major north dipping ductile shear zones or fault systems [Gansser, 1964; Le Fort, 1975, 1996; Hodges, 2000; Yin, 2006]. The Main Boundary Thrust (MBT) limits the LHS to the south, placing it over Neogene syn-tectonic detrital sedimentary rocks of the Siwalik Group. The Main Central Thrust (MCT) places GHS rocks over the LHS, and the syn-contractual top-to-the-north STDS separates the GHS from the TSS to

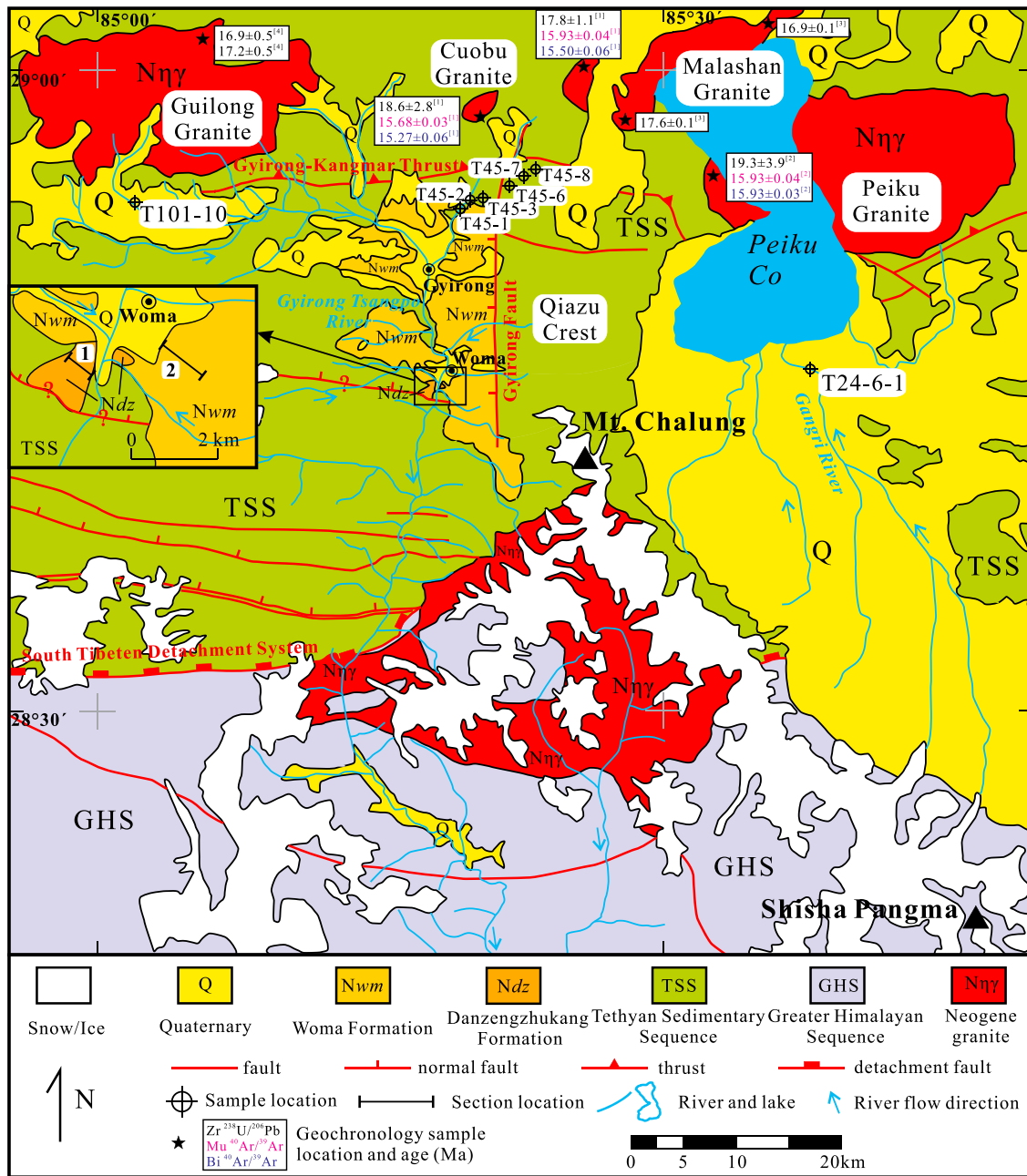


**Figure 3.** Simplified geologic map of the Gyirong basin and surrounding area, showing major lithotectonic units, fault systems, and sampling sites. Modified from Geological Map of Gyirong County (1:250,000) [Zhang, 2002]. Sample locations for this study are indicated, as well as published geochronology data: [1] Aoya *et al.* [2005]; [2] Kawakami *et al.* [2007]; [3] Gao and Zeng [2014]; and [4] Larson *et al.* [2010]. Inset shows an enlarged map of the part of the Gyirong basin that has been interpreted to be bounded by an east-west normal fault and where we sampled the basin succession.

the north [e.g., Hodges *et al.*, 1996]. The TSS consists of a thick and nearly continuous lower Paleozoic to Paleogene marine sedimentary succession, comprising sandstones, limestones, quartzites, shales, and slates [Garzanti *et al.*, 1986, 1987; Brookfield, 1993; Critelli and Garzanti, 1994; Liu and Einsele, 1994; Garzanti, 1999]. The GHS comprises Late Proterozoic to Early Cambrian high-grade metasediments and orthogneiss [Le Fort, 1975; Grujic *et al.*, 2002], along with Miocene leucogranite intrusions [e.g., Guillot *et al.*, 1993].

The Gyirong basin is located in the TSS and lies between the Thakkhola graben to the west and the Kung Co graben to the east. It is bounded by faults that are associated with the STDS to the south and the

Gyirong-Kangmar Thrust (GKT) to the north (Figures 2 and 3). North of the GKT, the Malashan, Peiku, Cuobu, Guilong (also called Kung Tang [Larson *et al.*, 2010]), and Changgo granites (Figures 2 and 3) belong to the North Himalayan Gneiss domes (NHGD) that stretch from east of the Kangmar dome to west of the Thakkola graben (Figure 1). Zircons from the Guilong, Malashan, Peiku, and Cuobu granites yield old ( $\geq 200$  Ma) (U-Th)/Pb core ages and Miocene rim ages (26–13.7 Ma) [Aoya *et al.*, 2005; Kawakami *et al.*, 2007; Larson *et al.*, 2010; Gao and Zeng, 2014], while muscovite, biotite, and K-feldspar  $^{40}\text{Ar}/^{39}\text{Ar}$  ages range between 15.9 and 15.3 Ma [Aoya *et al.*, 2005; Kawakami *et al.*, 2007]. These age patterns have been interpreted as recording intrusion of the granites between  $\sim 18.5$  and  $\sim 15.3$  Ma, followed by rapid cooling below  $\sim 300^\circ\text{C}$  before 15 Ma [Aoya *et al.*, 2005; Kawakami *et al.*, 2007]. From petrologic and structural studies, the same authors suggest that granite intrusion took place at  $\sim 18$  km depth ( $4.8 \pm 0.8$  kbar) after a phase of top-to-the-south thrusting (D1) and at the onset of a phase of top-to-the-north normal faulting (D2) [Aoya *et al.*, 2005; Kawakami *et al.*, 2007]. Similarly, crystallization of the Changgo granite mainly occurred at  $23.5 \pm 1$  Ma, syntectonically with D1 top-to-the-south deformation [Larson *et al.*, 2010]. The northern boundaries of the Guilong and Changgo granites correspond to a north dipping normal shear zone (D2) that is crosscut by undeformed dykes dated at  $16.6 \pm 0.3$  Ma [Larson *et al.*, 2010]. Muscovite and biotite  $^{40}\text{Ar}/^{39}\text{Ar}$  ages suggest that the dome cooled to below  $\sim 350^\circ\text{C}$  by  $\sim 17$  Ma and that D2 deformation stopped prior to 18.4 Ma [Larson *et al.*, 2010]. It thus appears that in the area, thickening coeval with or preceding granite emplacement was followed by Miocene extension, as in several other NHGD [Lee *et al.*, 2000, 2004; Aoya *et al.*, 2006; Quigley *et al.*, 2006].

South of the Gyirong basin, the lower STDS corresponds to mylonitic gneisses forming a  $\sim 6$  km thick, north dipping ductile shear zone [Yang *et al.*, 2009]. Two-mica granite intruded into the gneisses in the late Oligocene-early Miocene [Yang *et al.*, 2009]. Stretching lineations, rotated porphyroclasts, S-C fabrics, and asymmetric folds in the ductile shear zone consistently indicate a top-to-the-north movement. A series of north dipping normal faults affect the TSS, which have been interpreted as the upper STD controlling the initial development of basins in the Gyirong area [Burchfiel *et al.*, 1992; Hodges, 2000; Yang *et al.*, 2009].

The north-south trending GF bounds the Gyirong basin to the east (Figure 4a). This normal fault is outlined by brecciated rocks (Figure 4b) and expressed in the morphology as a prominent series of triangular facets along the eastern boundary of the basin (Figures 4a and 4c, see also Yang *et al.* [2009]). The fault dips about  $60^\circ$  ( $51^\circ$  to  $74^\circ$ ) to the west (N260–280°) [Yang *et al.*, 2009]. The large elevation difference between the Qiazu crest to the east of the fault, culminating at 6767 m (Mount Chalung), and the Neogene sedimentary basin to the west at  $\sim 4200$  m elevation reflects throw across the normal fault (Figures 3, 4a, and 4c). The height of the topographic facets is about 500 m, but the total offset could be much more, because of erosion of the hanging wall and deposition on the footwall during the Miocene-Pliocene. The GF crosscuts a series of east-west trending normal faults and folds in the Jurassic strata making up its footwall.

The GKT extends from Kangmar to the Gyirong area [Burg *et al.*, 1987] and is cut and offset by the GF as well as other north-south trending normal faults (Figures 2 and 3), such as that bounding the Kung Co half graben  $\sim 100$  km farther east [Mahéo *et al.*, 2007; Lee *et al.*, 2011]. Lee *et al.* [2000] suggest that thrusting along the GKT started at 15 Ma, whereas Lee *et al.* [2011] constrain normal faulting to have started on the Kung Co Fault at 12–13 Ma. If this timing is correct, it suggests that the GF was initiated after 15 Ma and possibly at 12–13 Ma, simultaneous with the Kung Co Fault.

## 2.2. Stratigraphy of the Gyirong Basin

The Neogene deposits of the Gyirong basin are divided into two units: the Danzengzhukang Formation (Figure 4d) and the Woma Formation (Figure 4e). We studied the basin fill in two sections to the south and southwest of the village of Woma, on the west and east side of the Gyirong Tsangpo, respectively (inset in Figure 3). A stratigraphic column is presented in Figure 5.

The Danzengzhukang Formation unconformably overlies Jurassic strata (Figure 4d), whereas its contact with the overlying Woma Formation is conformable. In the studied section (section 1, Figure 3), the Danzengzhukang Formation is 182 m thick and is composed of gray siliceous limestone, white quartzite, beige, salmon pink, and purple red sandstone pebbles, with lenticular sandstones and muddy siltstones (Figure 5). It contains plant fossils, pollen, molluscs, and ostracods [Xu *et al.*, 2012]. The Danzengzhukang Formation is interpreted to have been deposited in alluvial fan and braided-river environments [Xu *et al.*, 2012].

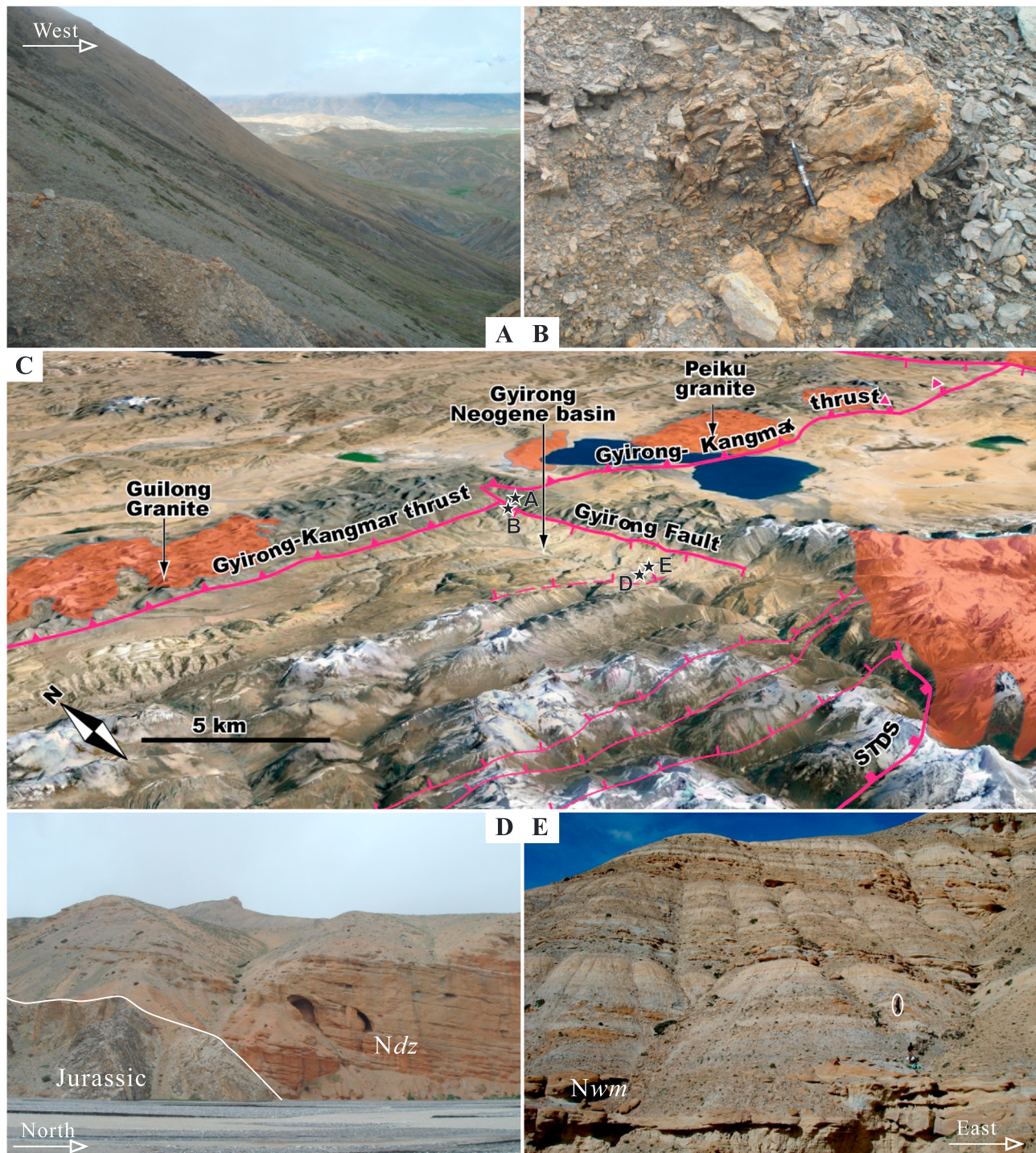


**Figure 4.** (a) Scarp of the Gyirong normal fault, showing the geomorphic contrast between the hanging wall and footwall of the fault. (b) Breccia in the fault zone, indicating extensive brittle fracturing. (c) Oblique Google Earth view from the SW, with the main faults and granites indicated, showing the relationship between the structure and the morphology. Locations of Figures 4a, 4b, 4d, and 4e are indicated. (d) Unconformable basal contact of the Neogene Danzengzhukang Formation (Ndz) on Jurassic strata. (e) View of the Neogene Woma Formation (Nwm). Person is highlighted by ellipse for scale.

The Woma Formation is 424 m thick in the studied section (section 2, Figure 3) and consists of conglomerates comprising siliceous limestone, granite, quartzite and sandstone pebbles, fine- to coarse-grained sandstones, siltstones, and mudstones (Figure 5). The Woma Formation deposits have been attributed to fan-delta and lacustrine depositional environments [Xu et al., 2012].

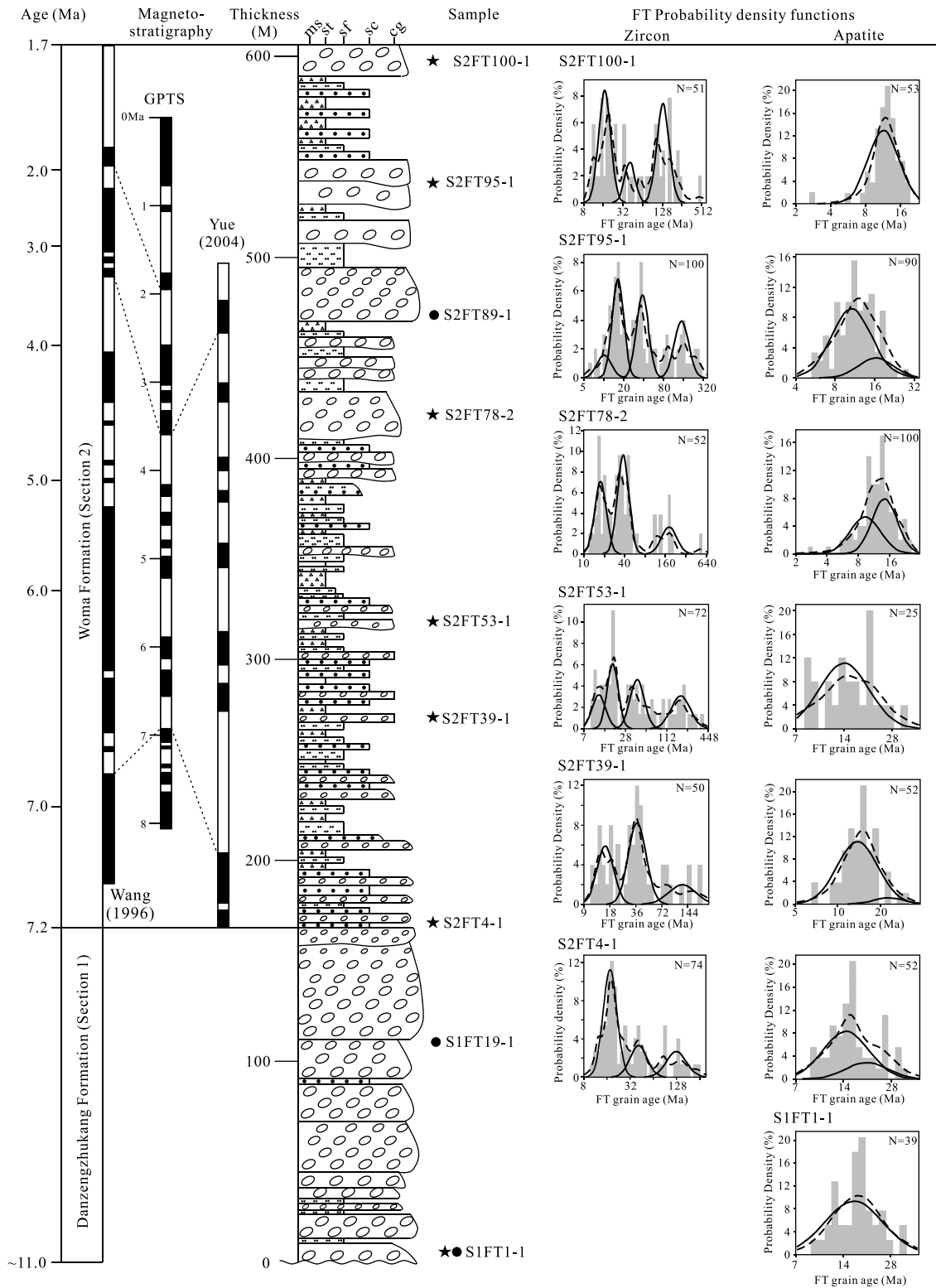


**Figure 5.** Stratigraphic column of the late Neogene sedimentary fill of the Gyirong basin measured in the field and fission-track age distribution of the samples (shown as histograms and probability density curves with fitted age populations). Lithology codes: ms, mudstone; st, siltstone; sf, fine sandstone; sc, coarse sandstone; and cg, conglomerate. GPTS: Geomagnetic Polarity Timescale [Cande and Kent, 1995], magnetostratigraphy data from Wang et al. [1996] and Yue et al. [2004]. Circle, zircon U-Pb sample and star, fission-track sample. Probability density functions and age populations for fission-track data are calculated using BinomFit [Brandon, 1992, 1996]. The dashed line is the single-grain age probability density function of the entire population; solid lines are modeled probability density functions for the fitted age populations; *N* is the number of dated grains. Detailed plots are shown in the supporting information (Figures S1 to S3).

The Woma Formation sequence has been dated magnetostratigraphically by Wang *et al.* [1996] and Yue *et al.* [2004]. The magnetostratigraphy includes reversals correlated with epochs between the lower Matuyama and Chron C3B [Wang *et al.*, 1996; Yue *et al.*, 2004], implying a depositional age for this formation between 7.2 and 1.7 Ma. In contrast, the age of the Danzengzhukang Formation is not well constrained. Assuming similar accumulation rates for the Woma and Danzengzhukang Formations would yield an initial depositional age of ~9.6 Ma for the Danzengzhukang Formation. This age is comparable to that (11–9.6 Ma) of the Tetang Formation, outcropping 130 km west of Gyirong in the Thakkhola graben [Garzzone *et al.*, 2003], which has lithofacies similar to that of the Danzengzhukang Formation [Adhikari and Wagreich, 2011] and is overlain by the Thakkhola Formation, with similar age and lithofacies as the Woma Formation [Garzzone *et al.*, 2003]. Therefore, we suggest the age of onset of sedimentation in the Gyirong basin to be around 10 Ma.

### 3. Sampling and Analytical Methods

#### 3.1. Sample Collection

Six samples of Jurassic metasandstone were collected across the GF, north of the Gyirong basin, with three samples coming from the footwall and three samples from the hanging wall. These samples were collected between 5282 and 4331 m elevation over a 6 km east-west horizontal distance, along a road that crosses the main fault plane near its northern tip (Figure 3). All of these samples were poor in apatite but rich in zircon, so we only report zircon fission-track ages for them.

Nine samples were collected for detrital U-Pb and fission-track analyses from the Neogene sedimentary succession of the Gyirong basin in the two studied sections (Danzengzhukang and Woma Formations, respectively; Figure 3). Two of the samples are from the Danzengzhukang Formation (S1FT1-1, S1FT19-1); the other seven samples (S2FT series) are from the Woma Formation (Figure 5). Samples S1FT1-1 and S1FT19-1 from the Danzengzhukang Formation and sample S2FT89-1 from the Woma Formation were selected for zircon U-Pb dating, in order to help constraining sediment provenance. The depositional age of samples from the Woma Formation can be determined by magnetostratigraphy with an error of  $\pm 0.5$  Ma [Wang *et al.*, 1996; Yue *et al.*, 2004] (see Table 2 and Figure 5). The depositional age of sample S1FT1-1, from the base of the Danzengzhukang Formation, is assumed to be  $10 \pm 1$  Ma.

Two samples were collected from modern river sands to assess recent patterns of exhumation. Sample T101-10 was collected from the Gyirong Tsangpo, west and upstream of the Gyirong basin (Figure 3). The catchment of this river mainly includes Jurassic sedimentary formations and the Miocene Guilong leucogranite, one of the North Himalayan intrusions. Sample T24-6-1 was collected farther east from the Gangri River, which is sourced from glaciers in the Shisha Pangma massif, within the GHS (Figure 3).

#### 3.2. Fission-Track Thermochronology

Fission-track samples were prepared for analysis by the external detector method [e.g., Tagami and O'Sullivan, 2005]. Both zircon fission-track (ZFT) and apatite fission-track (AFT) sample preparation and counting were performed at the State Key Laboratory of Geological Processes and Mineral Resources (GPMR), China University of Geosciences (Wuhan). Etching of polished zircon samples was carried out in a NaOH-KOH eutectic solution at a constant temperature of 228°C. We started with a short (1 h) etch and then etched the samples in 3 h increments until the tracks were abundant and clearly identifiable; total etching times varied from 19 to 31 h. Apatites were etched in 5 M HNO<sub>3</sub> at 22°C for 18 s. Although these conditions are slightly different from the standard (20 s at 21°C), this difference does not influence measured track densities and the effect on track lengths is minimal [Tagami and O'Sullivan, 2005]. Low-uranium mica was used as the external detector, and after irradiation these mica detectors were etched in 40% HF at room temperature for 18 min. Thermal neutron irradiation was carried out at the China Institute of Atomic Energy with a nominal thermal neutron fluence of  $1 \times 10^{15}$  cm<sup>-2</sup> for zircon and  $8 \times 10^{15}$  cm<sup>-2</sup> for apatite. ZFT and AFT counting was carried out under a magnification of 1000 (100 × 10) with a Zeiss microscope. Single-grain age populations and corresponding age peaks for each sample were determined using the binomial peak-fitting approach [Galbraith and Green [1990], Brandon [1996], see Stewart and Brandon [2004] for a detailed description]. Horizontal confined track lengths in apatite were measured using a Zeiss microscope at the State Key Laboratory of Continental Tectonics and Dynamics, Beijing, China.

### 3.3. Detrital Zircon U-Pb Geochronology

Zircon U-Pb dating was conducted by laser ablation multicollector inductively coupled plasma mass spectrometry at the GPMR, China University of Geosciences (Wuhan), using a spot diameter of 24  $\mu\text{m}$  or 32  $\mu\text{m}$ , depending on zircon crystal size. The data reduction procedures are described in *Liu et al.* [2008]. Zircon 91500 was used as the external standard for U-Pb dating and was analyzed twice for every six analyses [*Liu et al.*, 2010]. Time-dependent drifts of U-Th-Pb isotopic ratios were corrected using linear interpolation according to the variations of the external standard. To monitor age reproducibility and instrument stability, four GJ-1 zircon standards were inserted at the beginning and end of each run, making sure the results are consistent with recommended values [(608.5  $\pm$  0.4 Ma) *Jackson et al.*, 2004]. Each analysis incorporated a background acquisition of approximately 20–30 s (gas blank) followed by 50 s data acquisition from the sample. The Agilent Chemstation was used for the acquisition of individual analyses. Offline selection and integration of background and analyzed signals, time-drift correction, and quantitative calibration for trace-element analyses and U-Pb dating were performed by *ICPMSDataCal* [*Liu et al.*, 2008].

### 3.4. Data Analysis Methods

In order to link the cooling ages of sedimentary detritus with exhumation in the source terrain, we use the lag time concept. The lag time is defined as the difference between a thermochronological peak age and the depositional age of the sample [*Garver and Brandon*, 1994; *Garver et al.*, 1999; *Bernet et al.*, 2001]; it represents the time between closure of the thermochronologic system in the source and deposition in the adjacent basin [*Bernet and Garver*, 2005]. In active orogenic settings the time for sediment transport is negligible [e.g., *Bernet et al.*, 2004] and less than the resolution of the applied dating techniques. When plotting cooling ages against depositional ages in a lag time diagram, three basic lag time trends can be expected [*Bernet and Garver*, 2005]. A reduction of lag time up-section, which is regarded as a moving peak, indicates continuous and accelerating exhumation. Constant lag time means cooling ages become younger at the same rate as the change in depositional age, which is characteristic of a constantly exhuming source terrain and is also regarded as a moving peak. The third possible trend is that lag time increases and cooling-age peaks do not change up-section, which is described as a static peak and reflects an episode of rapid exhumation followed by slow erosion [*Bernet and Garver*, 2005; *Braun*, 2016].

## 4. Results

### 4.1. Detrital Zircon U-Pb Data

For each sample, 50 randomly selected single zircons were analyzed. Nonetheless, based on cathodoluminescence (CL) images, grains with complex uranium zoning were avoided [*Gehrels*, 2012]. The analytical data set is presented in the supporting information Table S1. Most analyses yielded concordant U-Pb ages (see the concordance data and plots in the supporting information Table S1 and Figure S4). We use  $^{206}\text{Pb}/^{238}\text{U}$  ages for zircons <1000 Ma and  $^{207}\text{Pb}/^{206}\text{Pb}$  ages for zircons >1000 Ma. The three samples show a similar age distribution, with single-grain U-Pb ages falling into two prominent age groups at ~500–600 and ~800–1250 Ma, and a number of less well-characterized peaks at ~1750, ~2000, and ~2300–2600 Ma (Figure 6). One of the 150 grains analyzed (S2FT89-1-16) yielded a Miocene  $^{206}\text{Pb}/^{238}\text{U}$  age (17  $\pm$  0.5 Ma; see Table S1).

### 4.2. Fission-Track Data

#### 4.2.1. Bedrock Fission-Track Data

Between 15 and 22 zircon grains were dated for the bedrock samples. Results are shown in Table 1. All samples passed the  $\chi^2$  test ( $P(\chi^2) > 5\%$ ). We report the ZFT ages as central ages, which are more robust against outliers [*Gallagher et al.*, 1998]. Five out of six ZFT ages are between 15.8  $\pm$  3.0 and 19.3  $\pm$  3.5 Ma (with an average of 17.4  $\pm$  1.1 Ma); sample T45-6, which was collected in the footwall closest to the fault plane, yields a younger age of 13.4  $\pm$  1.9 Ma. The ages show no correlation with elevation.

#### 4.2.2. Detrital Fission-Track Data

The objective was to date 100 grains per detrital sample in order to obtain statistically robust results [*Brandon*, 1996]. However, due to the scarcity of datable mineral grains, we could only count around 50 grains in several samples (Tables 2 and 3). Detrital fission-track ages are reported as central ages and binomial peak ages [*Brandon*, 1996; *Stewart and Brandon*, 2004] with  $\pm 2\sigma$  uncertainties in Tables 2 and 3. The probability density plots of the age populations for Neogene samples are shown in Figure 5. We also show radial plots and

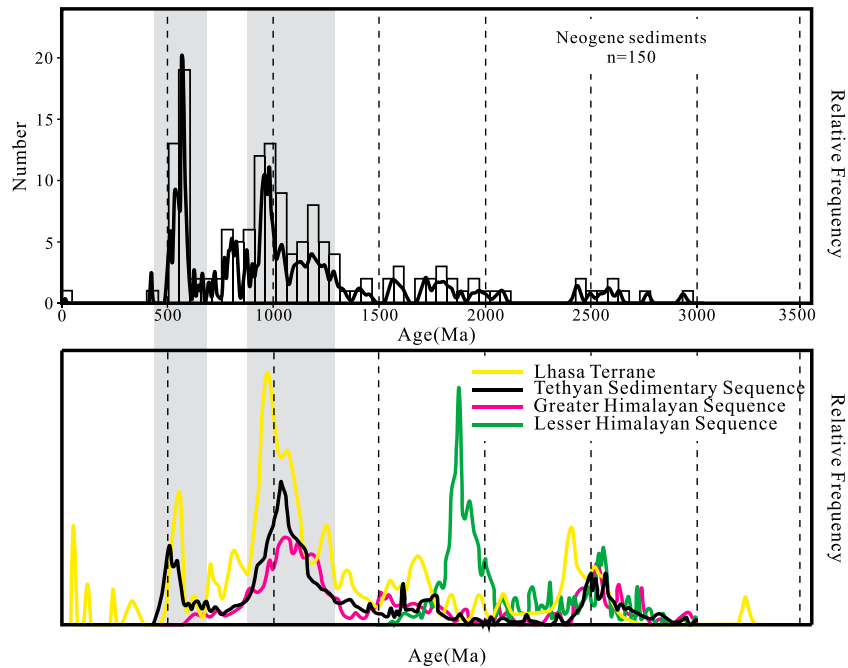


**Figure 6.** (top) Normalized probability density diagram (using Isoplot [Ludwing, 2012]) of detrital zircon U-Pb ages for Neogene sedimentary rocks of the Gyirong basin; the concordant and relative probability diagrams of individual samples are shown in the supporting information (Figure S4). (bottom) Detrital zircon U-Pb age populations of the main Himalayan sequences [DeCelles et al., 2004; Gehrels et al., 2011] and the Lhasa terrane [Kapp et al., 2007].

probability density plots together with the fitted age peaks for all samples in the supporting information (Figures S1 to S3).

All of the detrital ZFT samples failed the  $\chi^2$  test ( $P(\chi^2) < 5\%$ ) and are characterized by age dispersions  $D > 60\%$ , indicating that the ZFT age distributions contain multiple age populations [Brandon, 1992, 1996; van der Beek et al., 2006]. All ZFT age peaks are older than the corresponding depositional age of the sample, indicating that the detrital ZFT ages reflect the exhumation history in the source area rather than that of the basin. The different age components can thus be interpreted as reflecting source areas with variable denudation rates [Braun et al., 2006].

**Table 1.** Zircon Fission-Track Data for Jurassic Bedrock Samples Across the Gyirong Fault<sup>a</sup>

Sample	Location	Elevation (m)	Lithology	N	$\rho_s \times 10^6 \text{ cm}^{-2}$ ( $N_s$ )	$\rho_i \times 10^6 \text{ cm}^{-2}$ ( $N_i$ )	$\rho_d \times 10^5 \text{ cm}^{-2}$ ( $N_d$ )	$P(\chi^2)$ (%)	Central Age (Ma $\pm 2\sigma$ )	U (ppm)
T45-1	85.3167°E 28.8857°N	4331	Slate	19	2.32 (216)	3.34 (310)	3.753 (1758)	14.9	16.0 $\pm$ 3.0	354
T45-2	85.3317°E 28.9000°N	4410	Slate	15	2.41 (152)	3.49 (220)	3.795 (1793)	94.4	15.8 $\pm$ 3.0	366
T45-3	85.3467°E 28.9505°N	4536	Slate	22	2.44 (400)	3.24 (532)	3.815 (1810)	44.3	17.2 $\pm$ 2.2	339
T45-6	85.3678°E 28.9092°N	5123	Slate	22	2.69 (291)	4.65 (502)	3.857 (1845)	94.5	13.4 $\pm$ 1.9	480
T45-7	85.3761°E 28.9101°N	5184	Slate	20	2.85 (259)	4.01 (365)	3.898 (1880)	100	16.6 $\pm$ 2.5	410
T45-8	85.3808°E 28.9043°N	5282	Slate	15	3.09 (179)	3.79 (220)	3.94 (1915)	89.5	19.3 $\pm$ 3.5	383

<sup>a</sup>All samples were counted with a zeta calibration factor  $\zeta = 106.30 \pm 5.92$  for glass dosimeter CN1.  $N$  = total number of grains counted; binomial peak ages are given  $\pm 2$  SE (standard error). The percentage of grains in a specific peak is also given.  $P(\chi^2)$ ,  $\chi^2$  probability that the single-grain ages represent one population;  $D$ , age dispersion;  $N$ , number of horizontal confined track lengths measured; and MTL, mean track length.

**Table 2.** Detrital Zircon Fission-Track Results<sup>a</sup>

Sample	Location	Depositional Age (Ma)	N	Age Range (Ma)	$P(\chi^2)$ (%)	D (%)	P1 (Ma)	P2 (Ma)	P3 (Ma)	P4 (Ma)	Central Age (Ma)
T24-6-1	Gangri River	0	55	8.7–27.8	0.0	20.3	10.7 ± 1.2 30.6%	15.1 ± 1.3 62.1%	22.7 ± 4.8 7.3%	-	14.1 ± 1.2
T101-10	Gyirong Tsangpo	0	50	3.3–789.3	0.0	99.1	-	16.5 ± 1.2 64.0%	-	140.8 ± 16.1 36.0%	33.2 ± 9.5
S2FT100-1	Gyirong basin	1.7	51	10.7–481.1	0.0	90.2	-	16.8 ± 1.5 44.8%	40.8 ± 5.6 14.3%	131.9 ± 12.2 40.9%	42.3 ± 10.9
S2FT95-1	Gyirong basin	2.0	100	5.9–297.7	0.0	84.0	10.2 ± 2.3 10.0%	16.5 ± 1.6 34.2%	38.8 ± 3.4 30.7%	152.0 ± 15.3 25.1%	34.3 ± 6.0
S2FT78-2	Gyirong basin	4.1	52	12.1–523.4	0.0	66.9	-	17.8 ± 1.7 35.5%	38.2 ± 3.3 47.2%	181.6 ± 27.8 17.3%	36.1 ± 7.0
S2FT53-1	Gyirong basin	6.2	72	9.0–367.4	0.0	83.4	11.5 ± 1.7 18.1%	18.3 ± 1.9 29.1%	41.5 ± 4.8 27.5%	179.8 ± 26.3 25.3%	32.6 ± 6.7
S2FT39-1	Gyirong basin	6.7	50	11.4–211.4	0.0	62.0	-	16.0 ± 1.8 32.7%	37.5 ± 3.9 49.4%	125.5 ± 3.9 17.9%	32.8 ± 6.3
S2FT4-1	Gyirong basin	7.2	74	10.6–243.1	0.0	66.3	-	17.6 ± 1.5 58.7%	41.3 ± 6.9 21.2%	127.4 ± 18.9 200%	29.2 ± 4.9

<sup>a</sup>All samples were counted with a zeta calibration factor  $\zeta = 120.34 \pm 2.13$  for glass dosimeter CN1.  $N$  = total number of grains counted; binomial peak ages are given  $\pm 2$  SE. The percentage of grains in a specific peak is also given.  $P(\chi^2)$ ,  $\chi^2$  probability that the single-grain ages represent one population and  $D$ , age dispersion.

Using binomial peak fitting [Brandon, 1996; Stewart and Brandon, 2004], the detrital ZFT age distributions of each sample were decomposed into three or four distinct age populations (Table 2), which can be grouped in four peak-age groups that we term P1 to P4 (Figure 7). All samples from the Neogene sedimentary rocks contain a Mesozoic age peak (P4; 130–180 Ma), an Eocene peak (P3; 37–41 Ma), and a Miocene peak (P2; 15–18 Ma). Two samples also generate a 10–11 Ma peak (P1). If we pool all the grains as one sample, the result shows four age peaks at  $12.1 \pm 1.4$  (P1),  $17.9 \pm 1.3$  (P2),  $39.2 \pm 2.8$  (P3), and  $147.1 \pm 11.8$  Ma (P4), which is consistent with the age peaks shown by individual samples and gives us confidence in the deconvolution of age populations for individual samples, even those containing only ~50 single-grain ages. Both the P2 and P3 peak ages do not change significantly up-section (Figure 7), and they can, therefore, be considered as static peaks [Bernet and Garver, 2005]. Typically, 30–58% and 14–50% of dated grains fall into the P2 and P3 static age peaks, respectively. The population P4 contains a much older and broader range of ages; the associated age peak has a very large uncertainty in individual samples.

Detrital ZFT ages from the modern river sample T101-10 (Gyirong Tsangpo) can be divided into two populations with peak ages of  $16.5 \pm 1.2$  Ma and  $140.8 \pm 16.1$  Ma (Table 2). These two age peaks correspond to the P2 and P4 peaks of the detrital ZFT ages in the Neogene deposits (Table 2). Sample T24-6-1 (Gangri River) yields three ZFT age components, with peak ages of  $10.7 \pm 1.2$ ,  $15.1 \pm 1.3$ , and  $22.7 \pm 4.8$  Ma (Table 2). Whereas the two young age peaks correspond to the P1 and P2 peaks found in some samples from the Gyirong basin, the third peak does not correspond to any observed age peak in the sedimentary rocks.

In contrast to the detrital ZFT age distributions, three out of seven detrital AFT samples from the Neogene deposits are characterized by a single age population, with age dispersions  $D < 10\%$  and  $\chi^2$  probability  $P(\chi^2) > 5\%$  (Table 3). All other samples contain two age populations (Table 3 and Figure 8). The AFT peak ages and the central ages show a very clear exhumation trend with a 15–16 Ma peak (P2), similar to the ZFT P2 peak, present in all samples except the youngest one (although this peak age is not well defined in sample S2FT95-1, deposited at 2 Ma). An ~11 Ma age peak (P1), which is comparable to the ZFT P1 peak, is present in samples deposited after ~4 Ma. Two samples yield an age peak between 20 and 23 Ma (P3). We note, however, that the less-pronounced age peaks for the multiple-population samples always have a large error bar, resulting in a relatively small separation between the two peak ages. Therefore, we would not expect to resolve them in samples with smaller numbers of single-grain ages [e.g., Naylor et al., 2015].

The samples from modern river sands yield a central AFT age of  $11.9 \pm 1.8$  Ma (T101-10) and  $11.4 \pm 1.5$  Ma (T24-6-1), respectively (Table 3). Sample T24-6-1 contains a multiple age population, with two binomial peak-fit ages at  $4.6 \pm 5.7$  and  $11.6 \pm 1.5$  Ma.

**Table 3.** Detrital Apatite Fission-Track Results<sup>a</sup>

Sample	Location	Depositional Age (Ma)	N	Age Range (Ma)	$P(\chi^2)$ (%)	D (%)	P1 (Ma)	P2 (Ma)	P3 (Ma)	P4 (Ma)	Central Age (Ma)	n	MTL $\pm 1\sigma$ ( $\mu\text{m}$ )	Standard Deviation ( $\mu\text{m}$ )
T24-6-1	Gangri River	0	63	3.5–29.4	47.8	3.7	4.6 $\pm$ 5.7 2.3%	11.6 $\pm$ 1.5 97.7%	-	-	11.4 $\pm$ 1.5	-	-	-
T101-10	Gyirong Tsangpo	0	27	1.8–21.0	85.0	0.4	-	11.9 $\pm$ 1.8 100%	-	-	11.9 $\pm$ 1.7	-	-	-
S2FT100-1	Gyirong basin	1.7	53	1.8–18.9	95.2	0.4	-	11.5 $\pm$ 1.5 100%	-	-	11.5 $\pm$ 1.5	1	14.8	-
S2FT95-1	Gyirong basin	2.0	90	5.3–27.4	1.6	19.0	-	10.7 $\pm$ 1.9 80.3%	16.4 $\pm$ 7.8 19.7%	-	11.7 $\pm$ 1.6	23	14.1 $\pm$ 0.2	1.0
S2FT78-2	Gyirong basin	4.1	100	2.9–24.9	0.0	22.0	-	9.4 $\pm$ 2.0 44.6%	14.4 $\pm$ 2.5 55.4%	-	12.2 $\pm$ 1.6	16	13.9 $\pm$ 0.2	0.7
S2FT53-1	Gyirong basin	6.2	25	8.1–35.4	25.2	6.5	-	-	14.1 $\pm$ 2.3 100%	-	14.2 $\pm$ 2.5	-	-	-
S2FT39-1	Gyirong basin	6.7	52	6.6–29.8	31.2	11.1	-	-	13.8 $\pm$ 2.0 93.0%	23.2 $\pm$ 8.1 7.0%	14.5 $\pm$ 2.1	17	14.1 $\pm$ 0.2	0.9
S2FT4-1	Gyirong basin	7.2	52	9.0–36.9	19.6	12.3	-	-	15.1 $\pm$ 2.8 75.6%	20.8 $\pm$ 10.1 24.4%	16.5 $\pm$ 2.4	6	13.8 $\pm$ 0.2	0.5
S1FT1-1	Gyirong basin	10.0 $\pm$ 1.0	39	9.3–35.2	88.7	0.6	-	-	16.4 $\pm$ 2.6 100%	-	16.4 $\pm$ 2.4	-	-	-

<sup>a</sup>All samples were counted with a zeta calibration factor  $\xi = 106.30 \pm 5.92$  for glass dosimeter CN1. N = total number of grains counted; binomial peak ages are given  $\pm 2$  SE. The percentage of grains in a specific peak is also given.  $P(\chi^2)$ ,  $\chi^2$  probability that the single-grain ages represent one population; D, age dispersion; N, number of horizontal confined track lengths measured; and MTL, mean track length.

Horizontal confined apatite fission-track lengths could be measured in four detrital samples (between 6 and 23 individual track lengths measured); mean track lengths vary little between  $13.8 \pm 0.2$  and  $14.1 \pm 0.2 \mu\text{m}$  (Table 3). A single track length measured in the modern sample S2FT100-1 is  $14.8 \mu\text{m}$  (Table 3). Although insufficient track lengths could be measured for a quantitative interpretation, the overall relatively long measured lengths are characteristic of rapid cooling in the source area and absence of reheating of the samples since deposition [Gleadow *et al.*, 1986].

## 5. Discussion

### 5.1. Provenance of the Gyirong Neogene Sedimentary Rocks

The provenance of basin fills should differ strongly between supradetachment and rift basins [Friedmann and Burbank, 1995]. A supradetachment basin forms above a low-angle normal fault system, while a rift basin is usually bounded by steeper normal faults. In most supradetachment basins, primary drainages flow from the footwall across the detachment into the hanging wall, and the basin fill contains little detritus shed from the hanging wall [Friedmann and Burbank, 1995]. In an asymmetric rift basin system in contrast, where the hanging wall block is tilted toward the bounding fault, sediments are derived principally from the distal hanging wall block, as well as from rivers flowing along the axis of the rift [Schlische, 1991; Friedmann and Burbank, 1995]. Therefore, the provenance of the sediment fill in the Gyirong basin could help determining whether basin development was controlled by motion on normal faults associated with the STDS system or the GF.

Within the Danzengzhukang Formation, carbonate rocks dominate the composition of conglomerate pebbles, followed by quartzite and sand-

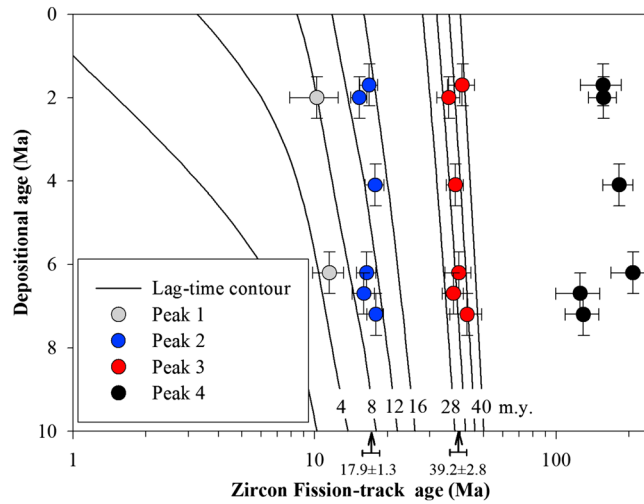


**Figure 7.** Lag time plot of detrital ZFT age peaks from the Gyirong basin sediments. Note the logarithmic scale used for the ZFT age axis. Error bars are  $\pm 2\sigma$  for FT ages and  $\pm 0.5$  Ma for depositional ages. The arrows illustrate the average ages of the P2 and P3 static peaks.

to the modern drainage system. The catchment of the modern Gyirong Tsangpo and its tributaries to the north of Woma is entirely within the Tethyan Himalayan belt (Figure 3). The similarity between the modern and fossil drainage systems suggests that the Neogene sedimentary rocks in the Gyirong basin should have been derived from the TSS.

A comparison of our detrital zircon U-Pb age distributions with published zircon U-Pb data from the TSS, GHS, LHS, and Lhasa terrane [DeCelles et al., 2000, 2004; Gehrels et al., 2011; Kapp et al., 2007] shows that the Neogene sedimentary rocks in the Gyirong basin display characteristic Tethyan zircon-age patterns (Figure 6 and Table S1). The lack of Cretaceous to Paleogene zircon U-Pb ages excludes a sedimentary source in the Lhasa terrane [DeCelles et al., 2007; Kapp et al., 2007]. Greater Himalayan detrital zircon U-Pb ages are broadly clustered about 1100 Ma, with smaller peaks at ~1500–1700 and ~2500 Ma [DeCelles et al., 2004]. Even though the granitic gneisses in the GHS yield zircons with U-Pb ages of 470–490 Ma [DeCelles et al., 2004],

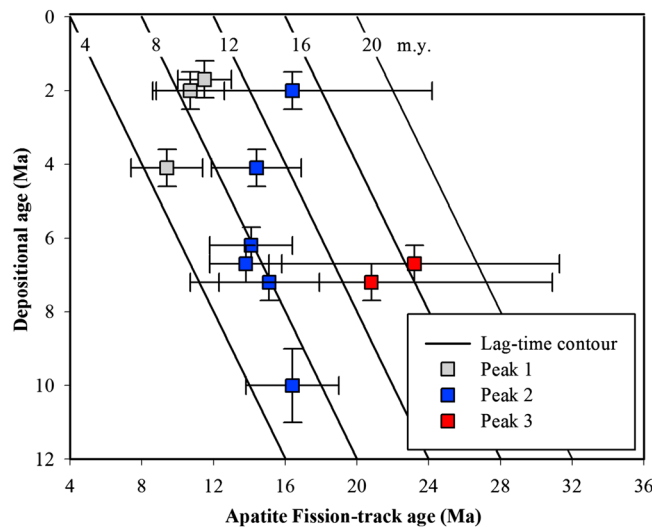


**Figure 8.** Lag time plot of detrital AFT age peaks from the Gyirong basin sediments. Error bars are  $\pm 2\sigma$  for FT ages and  $\pm 0.5$  Ma for depositional ages ( $\pm 1$  Ma for sample S1FT1-1).

stone clasts. Pebble imbrications indicate mostly southeast to east paleo-current directions [Xu et al., 2012]. In the Woma Formation, conglomerate clasts consist dominantly of quartzite, sandstone, granite, limestone, and slate; granitic clasts are absent before ~3.2 Ma [Xu et al., 2012]. Pebble imbrications and cross bedding show paleo-current directions toward the southwest and west [Xu et al., 2012]. The two sections are located to the west and east of the Gyirong Tsangpo trunk river, respectively (Figure 3). The paleo-current directions in the two sections correspond to the modern flow directions of the tributaries near them, implying that the paleo-drainage system during deposition of these formations between ~11 and 1.7 Ma was similar

to the modern drainage system. The catchment of the modern Gyirong Tsangpo and its tributaries to the north of Woma is entirely within the Tethyan Himalayan belt (Figure 3). The similarity between the modern and fossil drainage systems suggests that the Neogene sedimentary rocks in the Gyirong basin should have been derived from the TSS. A comparison of our detrital zircon U-Pb age distributions with published zircon U-Pb data from the TSS, GHS, LHS, and Lhasa terrane [DeCelles et al., 2000, 2004; Gehrels et al., 2011; Kapp et al., 2007] shows that the Neogene sedimentary rocks in the Gyirong basin display characteristic Tethyan zircon-age patterns (Figure 6 and Table S1). The lack of Cretaceous to Paleogene zircon U-Pb ages excludes a sedimentary source in the Lhasa terrane [DeCelles et al., 2007; Kapp et al., 2007]. Greater Himalayan detrital zircon U-Pb ages are broadly clustered about 1100 Ma, with smaller peaks at ~1500–1700 and ~2500 Ma [DeCelles et al., 2004]. Even though the granitic gneisses in the GHS yield zircons with U-Pb ages of 470–490 Ma [DeCelles et al., 2004], these ages do not form a significant peak compared to that at ~1100 Ma [DeCelles et al., 2000]. In the Tethyan sedimentary sequence, a ~1100 Ma age peak is also present, but the 500–600 Ma age peak is strongly developed [Gehrels et al., 2011], similar to the age spectrum yielded by the detrital zircons in the Gyirong basin (Figure 6). Only one 17.0 Ma zircon grain occurs in the youngest sandstone sample (S2FT89-1; depositional age ~3.8 Ma), which coincides with the appearance of granite pebbles in the upper part of the Neogene sedimentary section [Xu et al., 2012], indicating that erosion products of Miocene granites started contributing to the basin fill during the Pliocene.

Comparing the detrital thermochronology data with that from the

bedrock surrounding the basin and from modern river sands provides further constraints on sediment provenance. The Jurassic bedrock samples yield ZFT ages of  $\sim 16\text{--}19$  Ma, which is consistent with the major P2 peak (30–58% of single-grain ages) of the detrital ZFT age distributions from the Neogene sedimentary rocks. The Gyirong Tsangpo has its source in the Guilong granite, located northwest of the Gyirong basin (Figure 3), and sample T101-10 was collected from the river upstream of the Gyirong basin. The ZFT peak ages ( $16.5 \pm 1.2$  and  $140.8 \pm 16.1$  Ma) of this sample are consistent with the P2 and P4 ZFT age peaks from Neogene sedimentary rocks in the Gyirong basin, whereas the AFT age (a single population with a central age of  $11.9 \pm 1.8$  Ma) is similar to that of the samples from Neogene sedimentary rocks deposited after 4.1 Ma. The other modern river-sand sample, T24-6-1 collected in the Gangri River downstream of the Shisha Pangma, shows a ZFT age pattern that is distinctly different from that of the detrital samples from the Gyirong basin: a  $22.7 \pm 4.8$  Ma ZFT age peak that does not correspond to any observed ZFT age peaks in the Gyirong sedimentary rocks and a large  $10.7 \pm 1.2$  Ma ZFT age peak (Table 2). The age peaks encountered in sample T24-6-1 are instead consistent with the postemplacement cooling history of the early Miocene Shisha Pangma leucogranite in the GHS, which is the source of the modern Gangri River and cooled rapidly after crystallizing at  $\sim 20.2$  Ma down to the AFT closure temperature at  $\sim 14.8\text{--}11.9$  Ma [Searle *et al.*, 1997]. The different age structure of the sandstone samples and the modern Gangri River sample imply that the source of the Neogene sedimentary rocks of the Gyirong basin was not the GHS. Thus, the ZFT age analysis is consistent with the U-Pb data and supports the conclusion that the main source for the Neogene Gyirong basin fill is the TSS. Neogene leucogranites of the NHGD became a significant sediment source only during the Pliocene.

If sedimentation in the Gyirong basin were related to low-angle normal faulting linked with the STDS, one would expect the sediments to be derived from the footwall of the STDS, that is, the GHS to the south of the basin. However, this is not the case. Therefore, sedimentation in the Gyirong basin during the late Neogene appears unrelated to movement along normal faults linked to the STDS, but rather to normal faulting along the north-south trending GF since  $\sim 11$  Ma. This is in accordance with the N-S elongated shape of the basin, bounded to the east by the GF. The presence of an E-W normal fault bounding the Danzengzhukang formation to the south would suggest that the initial stage of basin formation could have resulted from low-angle normal fault movement linked with the STDS [Burchfiel *et al.*, 1992]. However, that fault is contentious and does not appear on the geological map of the area [Zhang, 2002]. Furthermore, as shown above, there appear to have been no major changes in the source of the sediments throughout the depositional history of the basin. We therefore suggest that all Neogene sedimentary rocks are linked to E-W extension since  $\sim 10$  Ma, consistent with the end of motion on the STDS at  $\sim 13\text{--}11$  Ma in this area [e.g., Leloup *et al.*, 2010].

## 5.2. Geodynamic Significance of the Detrital FT Record in the Neogene Gyirong Basin

The ZFT ages from the Neogene Gyirong basin show three clearly defined age peaks at  $17.9 \pm 1.3$  (P2),  $39.2 \pm 2.8$  (P3), and  $130\text{--}180$  Ma (P4); an  $\sim 11$  Ma peak (P1) is shown by two samples (Figures 5 and 7).

Sedimentary rocks of the TSS range from Ordovician to Cretaceous in age. Wang *et al.* [2010] reported a  $\sim 189$  Ma ZFT central age from a Jurassic TSS sandstone sample in the hanging wall of the Nyalam detachment (see location in Figure 2), which is compatible with our oldest ZFT age peak. Therefore, the P4 age component probably corresponds to zircons with pre-Himalayan cooling ages derived from nonmetamorphic TSS rocks.

The Eocene ZFT age peak P3 ( $39.2 \pm 2.8$  Ma) is younger than the depositional age of the TSS sedimentary rocks but older than the oldest Cenozoic U-Pb zircon ages found in the NHGD ( $35.0 \pm 0.8$  Ma in Mabja dome [Lee and Whitehouse, 2007] and  $35.4 \pm 0.4$  Ma in Changgo dome [Larson *et al.*, 2010]). These latter ages are interpreted as recording the onset of granite emplacement in the NHGD [Lee and Whitehouse, 2007; Larson *et al.*, 2010]. Crouzet *et al.* [2007] report peak temperatures in TSS rocks of around  $250\text{--}300^\circ\text{C}$ ,  $320\text{--}350^\circ\text{C}$ ,  $330\text{--}370^\circ\text{C}$ , and  $400\text{--}450^\circ\text{C}$  in the western Dolpo, Hidden Valley, Manang, and Marpha areas, respectively (see locations in Figures 1 and 2). Farther east, metamorphic peak temperatures could reach up to  $\sim 500^\circ\text{C}$  in the Bhutan TSS [Kellett *et al.*, 2009; Kellett and Grujic, 2012; Antolin *et al.*, 2012]. In the Manang and Hidden Valley areas, illite K/Ar data suggest that metamorphism took place around  $25\text{--}30$  Ma [Crouzet *et al.*, 2007]. A comparable age ( $27\text{--}30$  Ma) is suggested by Coleman [1998] in the Marsyandi Valley (see location in Figure 2). In the western part of the Himalaya, K/Ar ages from the TSS sequence are older:  $44\text{--}47$  Ma in

Zanskar, 42–45 Ma in Spiti, and ~41.5 Ma in Malari [Bonhomme and Garzanti, 1991; Wiesmayr, 2000; Wiesmayr and Grasmann, 1999; Williams *et al.*, 2001]. It thus appears that metamorphic temperatures sufficient to reset the ZFT system have affected various parts of the southern TSS between ~47 and ~27 Ma. Our preferred interpretation of the ~39 Ma ZFT age peak is that it corresponds to zircons sourced from metamorphosed parts of the TSS during the middle Eocene to early Oligocene shortening and crustal thickening within the Tethyan Himalayan thrust belt [e.g., Murphy and Yin, 2003], but the lack of detailed studies on metamorphism of TSS rocks near Gyirong precludes a more comprehensive interpretation.

The most intriguing aspect of the detrital ZFT age distribution is the major static age peak P2 at  $17.9 \pm 1.3$  Ma (Figure 7) and the corresponding 15–16 Ma AFT P2 age peak and central ages (Figure 8). The simplest scenario for generating such a peak would be that it corresponds to zircons (and apatites) derived from the Miocene North Himalayan granites outcropping north of the basin (Guilong, Cuobu, Malashan, and Peiku; Figure 3), as these leucogranites are known to have crystallized between ~23.1 and ~15.3 Ma, and cooled to ~350°C before ~15 Ma [Aoya *et al.*, 2005; Kawakami *et al.*, 2007; Larson *et al.*, 2010]. However, the provenance analysis discussed above indicates that granite-derived detritus first appeared only in the upper part of the Woma Formation at ~3.8 Ma [Xu *et al.*, 2012; this study], ruling out this provenance for the older sedimentary rocks. Furthermore, coincidence between the P2 ZFT age peak ( $17.9 \pm 1.3$  Ma) in the detrital record with the ZFT ages from the TSS bedrock (average  $17.4 \pm 1.1$  Ma) suggests that this peak is made up of reset zircons from the TSS.

Intrusion of Neogene granites should have led to widespread heating by contact metamorphism and resetting of the zircon and apatite fission-track systems in the TSS. The estimated emplacement pressure for the Cuobu granite is  $4.8 \pm 0.8$  kbar [Kawakami *et al.*, 2007], corresponding to a depth of ~18 km. This midcrustal depth implies that the granites and surrounding country rocks have not only cooled but have been significantly exhumed since the early Miocene. We thus suggest that the  $17.9 \pm 1.3$  Ma ZFT peak age and 15–16 Ma AFT ages not only reflect a rapid cooling event subsequent to granite emplacement but also rapid exhumation. The north dipping normal fault bounding the Changgo dome to the north was active between  $\sim 22.1 \pm 0.2$  and  $\sim 18.4$  Ma [Larson *et al.*, 2010]. In the Cuobu and Malashan domes, normal faulting was active from ~16 to ~15 Ma [Aoya *et al.*, 2005]. Such normal faults have triggered rapid cooling of the footwall resulting from up to 9 km of exhumation according to P-T estimates [Kawakami *et al.*, 2007]. A plausible source for the Mio-Pliocene Gyirong basin fill would be TSS rocks of the NHGD reset at the time of granite emplacement and cooled at the time of normal faulting on the northern margin of the domes. Final exhumation of these rocks would have taken place in the hanging of the GKT [Larson *et al.*, 2010] between ~15 Ma [Lee *et al.*, 2000] and ~12 Ma, prior to the onset of the N-S normal faults [Lee *et al.*, 2011]. However, sedimentation in the Gyirong basin started later, at ~10 Ma, and the bedrock samples located in the footwall of the GKT also show the ~17 Ma cooling event. This implies that the source of the Gyirong basin sediments is not restricted to the NHGD in the GKT hanging wall but includes large parts of the GKT footwall. In turn, this implies that the area affected by the ~17 Ma cooling event is not restricted to the NHGD but covers a larger area.

Rapid exhumation during ~18–15 Ma has also been reported by studies in several other locations within the collision belt, as well as in detrital deposits of the Himalayan foreland basin and Bengal submarine fan [e.g., Copeland and Harrison, 1990; Bernet *et al.*, 2006; Najman, 2006; Clift, 2006; Clift *et al.*, 2008]. In the Gangdese batholith west of Lhasa, exhumation between ~22 and 16 Ma has been documented from Gangdese arc rocks and conglomerates in the Kailas basin [Copeland *et al.*, 1995; Dai *et al.*, 2013; Carrapa *et al.*, 2014]. East of Lhasa, Tremblay *et al.* [2015] document a phase of rapid exhumation exceeding 1 km/Ma from 17–16 to 12–11 Ma, followed by very slow exhumation to the present. Nearby that study, in the Zedang area, Li *et al.* [2015] document a rapid cooling episode between circa 20 Ma and 15 Ma. Note that, although widespread, this phase of rapid exhumation is not recorded everywhere within the southern TSS: limited AFT ages from Paleocene TSS rocks in the Tingri region north of Everest are  $>42$  Ma [Najman *et al.*, 2010]. Within the northern GHS, a phase of rapid cooling and exhumation has been identified between ~17.5 and 15 Ma in Nyalam and between ~18 and 14 Ma in the Everest region [Leloup *et al.*, 2015; Orme *et al.*, 2015]. In the foreland of the Himalaya, ZFT ages from the Siwalik Group in Western Nepal contain a prominent static age peak at  $16 \pm 1.4$  Ma [Bernet *et al.*, 2006]. The latter two data sets have been interpreted as recording cessation of rapid exhumation of the GHS within the footwall of the STDS [Leloup *et al.*, 2015; Orme *et al.*, 2015; Braun, 2016]; however, the widespread occurrence of similar thermochronologic ages in the hanging wall and well to the north of the STDS (cf. above) suggests an additional or alternative mechanism. The northern limit of this

regional early Miocene exhumation could be the northern edge of the Gangdese batholith, because thermochronology data from the Lhasa terrane show much older cooling ages of  $>45$  Ma [Hetzl *et al.*, 2011; Rohrmann *et al.*, 2012; Haider *et al.*, 2013]. Therefore, the question is what triggered such regional exhumation in a widespread region during this period.

Carrapa *et al.* [2014] showed that the early Miocene Kailas conglomerates were buried to  $\sim 4$ – $7$  km depth before being exhumed rapidly at  $\sim 17$  Ma. They invoked renewed underthrusting of Indian lithosphere following a slab break-off event, thought to have occurred during the early Miocene [DeCelles *et al.*, 2011], to account for this rapid inversion of the Kailas basin. Lithosphere delamination beneath Central Tibet may have increased the mean elevation of the plateau by  $\sim 1$  km between 20 and 10 Ma [e.g., Molnar and Stock, 2009]; however, it would not have affected the Himalaya. From the analysis of global  $P$  wave tomography, slab detachment of the Indian lithosphere has been inferred to end at  $\sim 15$  Ma [e.g., Replumaz *et al.*, 2010]. Such detachment is followed by a phase where the northward moving Indian plate overrides the sinking slab. Husson *et al.* [2014] suggested that such a scenario could generate a dynamic deflection of the topography that would migrate southward. As a result, the Ganges foreland basin would have experienced rapid subsidence between 20 and 10 Ma, while the Himalaya and southern Tibet would show uplift. Such an evolutionary history is compatible with the suggestion of Mugnier and Huyghe [2006], who proposed that the Ganges basin geometry records significant uplift of the central Himalaya shortly before  $\sim 15$  Ma, controlled by break-off of the Indian continental lithosphere. Several numerical modeling studies demonstrate that slab break-off could lead to a maximum surface uplift of 2–6 km [Buiter *et al.*, 2002; Göğüş and Pysklywec, 2008] and to uplift of  $>1$  km in a 300 km wide area [Gerya *et al.*, 2004; Husson *et al.*, 2014]. The erosional response to such rapid and widespread surface uplift would cause considerable exhumation. As suggested by Husson *et al.* [2014], this phase of uplift and exhumation would mainly affect the northern Himalaya and southern Tibet, the region in which widespread thermochronological ages of 15–20 Ma occur. It would also precede the rapid exhumation on the southern flank of the Himalaya caused by overthrusting along the Main Himalayan Thrust [e.g., Bollinger *et al.*, 2004; Robert *et al.*, 2009; Herman *et al.*, 2010; Coutand *et al.*, 2014]; both the detrital thermochronological record from the southern Himalayan foreland basin [Bernet *et al.*, 2006] and numerical modeling inferences [Herman *et al.*, 2010; Coutand *et al.*, 2014] imply that this system has been active since  $\sim 10$ – $15$  Ma. We will discuss the differences between the northern and southern flanks of the Himalaya further in the next section.

A potential alternative explanation would link exhumation to continued underthrusting of India below Asia, leading simultaneously to E-W extension [Kapp and Guynn, 2004]. However, if the 15–18 Ma exhumation is linked to E-W extension resulting from insertion of Indian crust below Tibet [Kapp and Guynn, 2004], then such exhumation ages should be observed in both central and southern Tibet, considering the distribution of N-S rifts. However, thermochronological studies in the northern Lhasa terrane reported significantly older cooling ages, as mentioned above. Furthermore, most of the rifting took place after  $\sim 14$  Ma (see Sundell *et al.* [2013] for a review), which is later than the phase of rapid exhumation of TSS. Therefore, we suggest that the rapid and widespread early Miocene exhumation in the Himalaya and southern Tibet could be the response to dynamic rebound of the previously deflected topography of this region after slab break-off [Husson *et al.*, 2014].

All AFT samples of detrital sedimentary rocks deposited after  $\sim 4.1$  Ma, as well as the two modern river-sand samples, show central or peak ages of  $\sim 11$  Ma (Table 3 and Figure 8). This peak is also present in two detrital ZFT samples (Table 2). Such an apparently static peak could result from a major cooling event at  $\sim 11$  Ma; the most likely mechanism for such cooling would be footwall exhumation following initiation of the N-S trending GF. However, the AFT age peak of  $\sim 11$  Ma is also recorded by the two modern river samples, which were sourced from areas distinct from the footwall of the GF and of any other N-S trending faults (Figure 3). An alternative explanation for the absence of AFT ages younger than 11 Ma would therefore be that exhumation rates slowed down significantly in the TSS after  $\sim 11$  Ma [Bernet and Garver, 2005]. Given the relatively widespread extent of these ages, without a particular relationship to any geological structure, we prefer this latter interpretation.

The absence of significant local exhumation after 11 Ma could appear in contradiction with the fact that the Gyirong normal fault is clear in the morphology and bounds a graben filled with sedimentary rocks younger than  $\sim 11$  Ma. One should expect the footwall block of the fault, the Qiazu crest, to have been constantly

exhumed to yield the sediments filling the Gyirong basin. The lack of cooling ages younger than 11 Ma indicates that the footwall block of the fault has not yet been exhumed from depths sufficient to partially reset the AFT system. Assuming a geothermal gradient range of 15–50°C/km [Lee *et al.*, 2011] and a minimum AFT partial annealing temperature of 60°C [e.g., Gallagher *et al.*, 1998], this corresponds to less than 4000–1200 m of exhumation. The maximum vertical offset (MVO) of the GF can be estimated as the sum of the basin depth (thickness of the Neogene sedimentary deposits in the Gyirong basin; ~600 m), the relief between the surface of the basin and the summit of the footwall topography (Qiazu crest, 6800 m–4200 m = 2600 m) and the exhumation of the footwall. If the latter is less than 4000–1200 m, the MVO is less than 4400–7200 m. For a fault dip of 51–74° [Yang *et al.*, 2009] and continuous motion since ~10 Ma, these values correspond to a vertical throw rate of less than ~0.44–0.72 mm/yr, a slip rate of less than ~0.46–0.93 mm/yr, and an extension rate of less than ~0.13–0.58 mm/yr.

### 5.3. Differential Exhumation Between the Greater and Tethyan Himalaya

A complete understanding of the evolution of the Himalayan orogen requires knowledge of its exhumation history. However, even though the TSS constitutes an important component of the Himalayan orogen, thermochronological data for its exhumation remain relatively limited. In contrast, thermochronological data in the GHS are abundant, in particular for the central Himalaya, including detrital [Bernet *et al.*, 2006; van der Beek *et al.*, 2006; Chirouze *et al.*, 2012; Szulc *et al.*, 2006] and bedrock AFT and (U-Th)/He [e.g., Searle *et al.*, 1997; Huntington *et al.*, 2006; Blythe *et al.*, 2007; Robert *et al.*, 2009; Wang *et al.*, 2010; Li *et al.*, 2013] or  $^{40}\text{Ar}/^{39}\text{Ar}$  [e.g., Herman *et al.*, 2010] data (Figure 2). Our new data provide the opportunity to compare the exhumation history between the northern and southern flank of the central Himalaya, in order to improve our understanding of exhumation processes.

The most significant difference between the northern and southern flanks of the central Himalaya is that the southern flank is characterized by continuing rapid exhumation due to overthrusting over the Main Himalayan Thrust, leading to widespread young thermochronological ages [e.g., Blythe *et al.*, 2007; Robert *et al.*, 2009; Herman *et al.*, 2010; Thiede and Ehlers, 2013]. This difference is reflected by a 4 Myr lag time ZFT age peak recorded in the Siwaliks of western and central Nepal [Bernet *et al.*, 2006] but absent in the detrital thermochronological record of the Gyirong basin. The 4 Myr lag time peak appears in the Siwalik record at ~11 Ma, implying onset of rapid exhumation of part of the source area (comprising the GHS and LHS as well as part of the TSS) after 15 Ma at a rate of  $1.4 \pm 0.2$  km/Myr [Bernet *et al.*, 2006]. This timing thus closely follows the widespread ~15–18 Ma regional cooling and exhumation in the southern Tibetan Plateau and the Himalaya. In contrast, our detrital ZFT and AFT data from the Gyirong basin imply that exhumation slowed after 16–17 Ma, as also evidenced in the Kailas basin and the Gangdese batholith [Carrapa *et al.*, 2014; Dai *et al.*, 2013; Tremblay *et al.*, 2015].

Although on a local scale, this difference in exhumation patterns can be related to motion on the STDS, which resulted in rapid rock uplift of the footwall, i.e., the northern GHS, and stability or subsidence in its hanging wall, i.e., the TSS, the widespread regional patterns of contrasting ages and the timing suggest additional or alternative mechanisms. An alternative explanation would involve the onset of strongly varying erosion intensity between the two flanks of the Himalaya due to installation of the strong orographic gradient that characterizes the modern mountain belt [e.g., Bookhagen and Burbank, 2006]. Only little monsoonal precipitation nowadays penetrates into the orogen along major river valleys [Thiede *et al.*, 2004], rendering erosion and exhumation in the TSS inefficient. Increased exhumation rates on the southern Himalayan flank have been linked to strengthening of the Asian Monsoon in the early Miocene [Clift *et al.*, 2008]. However, modern erosion and exhumation rates on the southern Himalayan flank do not seem primarily controlled by climatic parameters [Godard *et al.*, 2014; Abrahami *et al.*, 2016], and estimates for the onset of aridity on different parts of the Tibetan Plateau vary widely, from late Eocene to late Miocene [e.g., Zhisheng *et al.*, 2001; Dettman *et al.*, 2003; Dupont-Nivet *et al.*, 2007].

The modern, southward propagating thrust system of the Himalaya, which controls the exhumation pattern on its southern flank [e.g., Blythe *et al.*, 2007; Robert *et al.*, 2009; Herman *et al.*, 2010; Coutand *et al.*, 2014], appears to have been installed since the early Miocene [e.g., DeCelles *et al.*, 1998; Mugnier and Huyghe, 2006]. Stable isotope paleoaltimetry based on the hydrogen isotope ratios ( $\delta D$ ) of hydrous minerals that were formed in the STDS shear zone during the early Miocene suggests that elevations on the order of 5000 m were reached in the Mount Everest area by ~17 Ma [Gébelin *et al.*, 2013]. Increasing sedimentation rates since

the Middle Miocene in the Himalayan foreland basin [Najman, 2006] reflect accelerating erosion and exhumation of the GHS and LHS. Conversely, sedimentation within the TSS zone after ~17 Ma was limited to local basins related to N-S normal faults, such as the Gyirong and Thakkhola basins. Therefore, we propose that differential exhumation after 17 Ma between the TSS and GHS results primarily from focused deformation on the southern flank, possibly aided by focused monsoon precipitation.

## 6. Conclusions

Neogene (~10–1.7 Ma) sedimentary rocks of the Gyirong basin in southern Tibet are derived from TSS rocks rather than the GHS, as shown by their detrital zircon U-Pb age signature as well as a comparison of their zircon and apatite fission-track age spectrum with bedrock and modern river-sand data. This provenance implies that development of the Gyirong basin is independent of low-angle normal faulting linked to the STDS but is rather controlled by the N-S trending GF that initiated at ~10 Ma.

The detrital ZFT thermochronology record shows three age peaks at  $17.9 \pm 1.3$  Ma,  $39.2 \pm 2.8$  Ma, and 130–180 Ma, which occur in all samples. Detrital AFT age peaks and central ages show a 15–16 Ma peak present until 2.0 Ma, as well as an ~11 Ma peak from 4.1 Ma to recent. Exhumation of the GF footwall has not been sufficient to bring rocks from the apatite fission-track partial annealing zone to the surface, suggesting that the total vertical throw is less than 4400–7200 m. However, fission-track ages shed light on previous cooling events that have occurred in the TSS. The 130–180 Ma and  $39.2 \pm 2.8$  Ma ZFT age peaks represent unreset TSS sources and TSS zircons that were reset during Eocene Himalayan metamorphism, respectively. The  $17.9 \pm 1.3$  Ma ZFT peak and 15–16 Ma AFT ages indicate widespread rapid cooling and exhumation of the TSS during this time. This early Miocene rapid exhumation is not limited to the TSS but is regional in scale, as it is also recorded in the Kailas basin and the southern Gangdese batholith to the north as well as the northern GHS to the south, and shows up in the detrital thermochronological record of the Himalayan foreland basin and the Bengal fan. Such widespread rapid exhumation can possibly be attributed to dynamic uplift of the Himalaya and southern Tibet, subsequent to break-off of the Indian subducting slab and overriding of the detached slab segment by the Indian plate. Subsequently, the detrital AFT ages illustrate that exhumation of the TSS slowed and appears to have stalled at ~11 Ma. In contrast, exhumation of the GHS and LHS remained active and may even have been enhanced after 16 Ma, due to the onset of the modern southward propagating thrust system on the southern Himalayan flank.

## Acknowledgments

This study was financially supported by the China Geological Survey (1212011121261), the National Natural Science Foundation of China (41202144), the Fundamental Research Funds for the Central Universities, China University of Geosciences (Wuhan) (G1323521545), and the China Scholarship Council. The manuscript was initiated during an extended stay by Tianyi Shen at ISTerre, Grenoble. Shen thanks Laurent Husson and Anne Replumaz from ISTerre for discussions about the mantle flow model. We also thank Li Haibing for helping in apatite fission-track length measurements. Comments by Editor Nathan A. Niemi, Associate Editors Djordje Grujic, Barbara Carrapa, and Kyle Larson, as well as two anonymous reviewers helped to clarify earlier versions of this manuscript. The DEM data set is provided by Geospatial Data Cloud, Computer Network Information Center, Chinese Academy of Sciences (<http://www.gscloud.cn>).

## References

- Abrahami, R., P. van der Beek, P. Huyghe, E. Hardwick, and J. Carcaillet (2016), Decoupling of long-term exhumation and short-term erosion rates in the Sikkim Himalaya, *Earth Planet. Sci. Lett.*, *433*, 76–88, doi:10.1016/j.epsl.2015.10.039.
- Adhikari, B. R., and M. Wagnreich (2011), Provenance evolution of collapse graben fill in the Himalaya—The Miocene to Quaternary Thakkhola-Mustang Graben (Nepal), *Sediment. Geol.*, *233*(1–4), 1–14, doi:10.1016/j.sedgeo.2010.09.021.
- Antolín, B., E. Schill, D. Grujic, S. Baule, X. Quidelleur, E. Appel, and M. Waldhör (2012), E-W extension and block rotation of the southeastern Tibet: Unravelling late deformation stages in the eastern Himalayas (NW Bhutan) by means of pyrrhotite remanences, *J. Struct. Geol.*, *42*, 19–33, doi:10.1016/j.jsg.2012.07.003.
- Aoya, M., S. R. Wallis, K. Terada, J. Lee, T. Kawakami, Y. Wang, and M. Heizler (2005), North-south extension in the Tibetan crust triggered by granite emplacement, *Geology*, *33*(11), 853–856, doi:10.1130/G21806.1.
- Aoya, M., S. R. Wallis, T. Kawakami, J. Lee, Y. Wang, and H. Maeda (2006), The Malashan gneiss dome in south Tibet: Comparative study with the Kangmar dome with special reference to kinematics of deformation and origin of associated granites, *Geol. Soc. London Spec. Publ.*, *268*, 471–495, doi:10.1144/GSL.SP.2006.268.01.22.
- Armijo, R., P. Tapponnier, J. L. Mercier, and T. L. Han (1986), Quaternary extension in southern Tibet: Field observations and tectonic implications, *J. Geophys. Res.*, *91*, 13,803–13,872, doi:10.1029/JB091iB14p13803.
- Bernet, M., and J. I. Garver (2005), Fission-track analysis of detrital zircon, *Rev. Mineral. Geochem.*, *58*, 205–237, doi:10.2138/rmg.2005.58.8.
- Bernet, M., M. Zattin, J. I. Garver, M. T. Brandon, and J. A. Vance (2001), Steady-state exhumation of the European Alps, *Geology*, *29*(1), 35–38, doi:10.1130/0091-7613(2001)029<0035:SSEOTE>2.0.CO;2.
- Bernet, M., M. T. Brandon, J. I. Garver, and B. Molitor (2004), Downstream changes of Alpine zircon fission-track ages in the Rhône and Rhine Rivers, *J. Sediment. Res.*, *74*(1), 82–94, doi:10.1306/041003740082.
- Bernet, M., P. van der Beek, R. Pik, P. Huyghe, J.-L. Mugnier, E. Labrin, and A. Szulc (2006), Miocene to recent exhumation of the central Himalaya determined from combined detrital zircon fission-track and U/Pb analysis of Siwalik sediments, western Nepal, *Basin Res.*, *18*, 393–412, doi:10.1111/j.1365-2117.2006.00303.x.
- Blythe, A. E., D. W. Burbank, A. Carter, K. Schmidt, and J. Putkonen (2007), Plio-Quaternary exhumation history of the central Nepalese Himalaya: 1. Apatite and zircon fission track and apatite [U-Th]/He analyses, *Tectonics*, *26*, TC3002, doi:10.1029/2006TC001990.
- Bollinger, L., J. Avouac, O. Beyssac, E. Catlos, T. Harrison, M. Grove, B. Goffé, and S. Sapkota (2004), Thermal structure and exhumation history of the Lesser Himalaya in central Nepal, *Tectonics*, *23*, TC5015, doi:10.1029/2003TC001564.
- Bonhomme, M., and E. Garzanti (1991), Age of metamorphism in the Zaskar Tethys Himalaya (India), *Geologic Alpine Memoirs*, *16*, 15–16.
- Bookhagen, B., and D. W. Burbank (2006), Topography, relief, and TRMM-derived rainfall variations along the Himalaya, *Geophys. Res. Lett.*, *33*, L08405, doi:10.1029/2006GL026037.

- Brandon, M. T. (1992), Decomposition of fission-track grain-age distributions, *Am. J. Sci.*, *292*(8), 535–564, doi:10.2475/ajs.292.8.535.
- Brandon, M. T. (1996), Probability density plot for fission-track grain-age samples, *Radiat. Meas.*, *26*(5), 663–676, doi:10.1016/S1350-4487(97)82880-6.
- Braun, J. (2016), Strong imprint of past orogenic events on the thermochronological record, *Tectonophysics*, doi:10.1016/j.tecto.2016.05.046.
- Braun, J., P. van der Beek, and G. Batt (2006), *Quantitative Thermochronology, Numerical Methods for the Interpretation of Thermochronological Data*, Cambridge Univ. Press, New York.
- Brookfield, M. E. (1993), The Himalayan passive margin from Precambrian to Cretaceous, *Sediment. Geol.*, *84*(1), 1–35, doi:10.1016/0037-0738(93)90042-4.
- Buiter, S. J. H., R. Govers, and M. J. R. Wortel (2002), Two-dimensional simulations of surface deformation caused by slab detachment, *Tectonophysics*, *354*(3), 195–210, doi:10.1016/S0040-1951(02)00336-0.
- Burchfiel, B. C., Z. Chen, K. V. Hodges, Y. Liu, L. H. Royden, C. Deng, and J. Xu (1992), The south Tibetan detachment system, Himalayan orogen: Extension contemporaneous with and parallel to shortening in a collisional mountain belt, *Geol. Soc. Am. Spec. Pap.*, *269*, 1–41, doi:10.1130/SPE269-p1.
- Burg, J. P., M. Brunel, D. Gapais, G. M. Chen, and G. H. Liu (1984), Deformation of leucogranites of the crystalline Main Central Sheet in southern Tibet (China), *J. Struct. Geol.*, *6*(5), 535–542, doi:10.1016/0191-8141(84)90063-4.
- Burg, J. P., A. Leyreloup, J. Girardeau, and G. M. Chen (1987), Structure and metamorphism of a tectonically thickened continental crust: The Yalu Tsangpo suture zone (Tibet), *Philos. Trans. R. Soc. Lond.*, *321*, 67–86.
- Cande, S. C., and D. V. Kent (1995), Revised calibration of the geomagnetic polarity timescale for the Late Cretaceous and Cenozoic, *J. Geophys. Res.*, *100*, 6093–6095, doi:10.1029/94JB03098.
- Carrapa, B., D. A. Orme, P. G. DeCelles, P. Kapp, M. A. Cosca, and R. Waldrip (2014), Miocene burial and exhumation of the India-Asia collision zone in southern Tibet: Response to slab dynamics and erosion, *Geology*, *42*, 443–446, doi:10.1130/G35350.1.
- Chirouze, F., M. Bernet, P. Huyghe, V. Erens, G. Dupont-Nivet, and F. Senebier (2012), Detrital thermochronology and sediment petrology of the middle Siwaliks along the Muksar Khola section in eastern Nepal, *J. Asian Earth Sci.*, *44*, 94–106, doi:10.1016/j.jseas.2011.01.009.
- Clift, P. D. (2006), Controls on the erosion of Cenozoic Asia and the flux of clastic sediment to the ocean, *Earth Planet. Sci. Lett.*, *241*(3), 571–580, doi:10.1016/j.epsl.2005.11.028.
- Clift, P. D., K. V. Hodges, D. Heslop, R. Hannigan, H. Van Long, and G. Calves (2008), Correlation of Himalayan exhumation rates and Asian monsoon intensity, *Nat. Geosci.*, *1*(12), 875–880, doi:10.1038/ngeo351.
- Cogan, M. J., K. D. Nelson, W. S. F. Kidd, and C. Wu (1998), Shallow structure of the Yadong-Gulu rift, southern Tibet, from refraction analysis of Project INDEPTH common midpoint data, *Tectonics*, *17*, 46–61, doi:10.1029/97TC03025.
- Colchen, M. (1999), The Thakkhola-Mustang graben in Nepal and the Late Cenozoic extension in the Higher Himalayas, *J. Asian Earth Sci.*, *17*, 683–702, doi:10.1016/S1367-9120(99)00037-1.
- Coleman, M. E. (1998), U-Pb constrains on Oligocene-Miocene deformation and anatexis within the central Himalaya, Marsyandi Valley, Nepal, *J. Sci.*, *298*, 553–571.
- Copeland, P., and T. M. Harrison (1990), Episodic uplift in the Himalaya revealed by <sup>40</sup>Ar/<sup>39</sup>Ar analysis of detrital K-feldspar and muscovite, Bengal fan, *Geology*, *18*, 354–357, doi:10.1130/0091-7613(1990)018<0354:ERUITH>2.3.CO;2.
- Copeland, P., T. M. Harrison, Y. Pan, W. S. F. Kidd, M. Roden, and Y. Zhang (1995), Thermal evolution of the Gangdese batholith, southern Tibet: A history of episodic unroofing, *Tectonics*, *14*, 223–236, doi:10.1029/94TC01676.
- Coutand, I., D. M. Whipp, D. Grujic, M. Bernet, M. G. Fellin, B. Bookhagen, K. R. Landry, S. Ghalley, and C. Duncan (2014), Geometry and kinematics of the Main Himalayan Thrust and Neogene crustal exhumation in the Bhutanese Himalaya derived from inversion of multi-thermochronologic data, *J. Geophys. Res. Solid Earth*, *119*, 1446–1481, doi:10.1002/2013JB010891.
- Critelli, S., and E. Garzanti (1994), Provenance of the lower Tertiary Murree redbeds (Hazara-Kashmir syntaxis, Pakistan) and the initial rising of the Himalayas, *Sediment. Geol.*, *89*(3), 265–284, doi:10.1016/0037-0738(94)90097-3.
- Crouzet, C., I. Dunkl, L. Paudel, P. Arkai, T. M. Rainer, K. Balogh, and E. Appel (2007), Temperature and age constraints on the metamorphism of the Tethyan Himalaya in Central Nepal: A multidisciplinary approach, *J. Asian Earth Sci.*, *30*(1), 113–130, doi:10.1016/j.jseas.2006.07.014.
- Dai, J., C. Wang, J. Hourigan, Z. Li, and G. Zhuang (2013), Exhumation history of the Gangdese batholith, Southern Tibetan Plateau: Evidence from apatite and zircon (U-Th)/He thermochronology, *J. Geol.*, *121*(2), 155–172, doi:10.1086/669250.
- DeCelles, P. G., G. E. Gehrels, J. Quade, T. Ojha, P. Kapp, and B. Upreti (1998), Neogene foreland basin deposits, erosional unroofing, and the kinematic history of the Himalayan fold-thrust belt, western Nepal, *Geol. Soc. Am. Bull.*, *110*(1), 2–21, doi:10.1130/0016-7606(1998)110<0002:NFBDEU>2.3.CO;2.
- DeCelles, P. G., G. E. Gehrels, J. Qade, B. LaReau, and M. Spurlin (2000), Tectonic implications of U-Pb zircon ages of the Himalayan orogenic belt in Nepal, *Science*, *288*(5465), 497–499, doi:10.1126/science.288.5465.497.
- DeCelles, P. G., G. E. Gehrels, Y. Najman, A. Martin, A. Carter, and E. Garzanti (2004), Detrital geochronology and geochemistry of Cretaceous–Early Miocene strata of Nepal: Implications for timing and diachroneity of initial Himalayan orogenesis, *Earth Planet. Sci. Lett.*, *227*(3), 313–330, doi:10.1016/j.epsl.2004.08.019.
- DeCelles, P. G., P. Kapp, L. Ding, and G. E. Gehrels (2007), Late Cretaceous to middle Tertiary basin evolution in the central Tibetan Plateau: Changing environments in response to tectonic partitioning, aridification, and regional elevation gain, *Geol. Soc. Am. Bull.*, *119*(5–6), 654–680, doi:10.1130/B26074.1.
- DeCelles, P. G., P. Kapp, J. Quade, and G. E. Gehrels (2011), Oligocene-Miocene Kailas basin, Southwestern Tibet: Record of postcollisional upper-plate extension in the Indus-Yarlung suture zone, *Geol. Soc. Am. Bull.*, *123*(7–8), 1337–1362, doi:10.1130/B30258.1.
- DeCelles, P. G., P. Kapp, G. E. Gehrels, and L. Ding (2014), Paleocene-Eocene foreland basin evolution in the Himalaya of southern Tibet and Nepal: Implications for the age of initial India-Asia collision, *Tectonics*, *33*, 834–849, doi:10.1002/2014TC003522.
- Dettman, D. L., X. Fang, C. N. Garzzone, and J. Li (2003), Uplift-driven climate change at 12 Ma: A long  $\delta^{18}O$  record from the NE margin of the Tibetan Plateau, *Earth Planet. Sci. Lett.*, *214*(1), 267–277, doi:10.1016/S0012-821X(03)00383-2.
- Dupont-Nivet, G., W. Krijgsman, C. G. Langereis, H. A. Abels, S. Dai, and X. Fang (2007), Tibetan Plateau aridification linked to global cooling at the Eocene-Oligocene transition, *Nature*, *445*(7128), 635–638, doi:10.1038/nature05516.
- Friedmann, S. J., and D. W. Burbank (1995), Rift basins and supradetachment basins: Intracontinental extensional end-members, *Basin Res.*, *7*, 109–127.
- Galbraith, R. (1990), The radial plot: Graphical assessment of spread in ages, *Nucl. Tracks Radiat. Meas.*, *17*(3), 207–214, doi:10.1016/1359-0189(90)90036-W.
- Galbraith, R., and P. Green (1990), Estimating the component ages in a finite mixture, *Nucl. Tracks Radiat. Meas.*, *17*(3), 197–206, doi:10.1016/1359-0189(90)90035-V.

- Gallagher, K., R. Brown, and C. Johnson (1998), Fission track analysis and its applications to geological problems, *Ann. Rev. Earth Planet. Sci.*, 26(1), 519–572, doi:10.1146/annurev.earth.26.1.519.
- Gansser, A. (1964), *The Geology of the Himalayas*, Wiley Intersci., New York.
- Gao, L.-E., and L. Zeng (2014), Fluxed melting of metapelite and the formation of Miocene high-CaO two-mica granites in the Malashan gneiss dome, southern Tibet, *Geochim. Cosmochim. Acta*, 130, 136–155, doi:10.1016/j.gca.2014.01.003.
- Garver, J. I., and M. T. Brandon (1994), Fission-track ages of detrital zircon from Cretaceous strata, southern British Columbia: Implications for the Baja BC hypothesis, *Tectonics*, 13, 401–420, doi:10.1029/93TC02939.
- Garver, J. I., M. T. Brandon, M. K. Roden-Tic, and P. J. J. Kamp (1999), Exhumation history of orogenic highlands determined by detrital fission track thermochronology, in *Exhumation Processes: Normal Faulting, Ductile Flow, and Erosion*, edited by U. Ring et al., *Geol. Soc. London Spec. Publ.*, 154, 283–304, doi:10.1144/GSL.SP.1999.154.01.13.
- Garzanti, E. (1999), Stratigraphy and sedimentary history of the Nepal Tethys Himalaya passive margin, *J. Asian Earth Sci.*, 17(5), 805–827, doi:10.1016/S1367-9120(99)00017-6.
- Garzanti, E., R. Casnedi, and F. Jadoul (1986), Sedimentary evidence of a Cambro-Ordovician orogenic event in the northwestern Himalaya, *Sediment. Geol.*, 48(3–4), 237–265, doi:10.1016/0037-0738(86)90032-1.
- Garzanti, E., A. Baud, and G. Mascle (1987), Sedimentary record of the northward flight of India and its collision with Eurasia (Ladakh Himalaya India), *Geodin. Acta*, 1(4–5), 297–312, doi:10.1080/09853111.1987.11105147.
- Garzanti, E., P. G. DeCelles, D. G. Hodkinson, T. P. Ojha, and B. N. Upreti (2003), East-west extension and Miocene environmental change in the southern Tibetan plateau: Thakkhola graben, central Nepal, *Geol. Soc. Am. Bull.*, 115(1), 3–20, doi:10.1130/0016-7606(2003)115<0003: EWEAME>2.0.CO;2.
- Gébelin, A., A. Mulch, C. Teysier, M. J. Jessup, R. D. Law, and M. Brunel (2013), The Miocene elevation of Mount Everest, *Geology*, 41(7), 799–802, doi:10.1130/G34331.1.
- Gehrels, G. (2012), Detrital zircon U-Pb geochronology: current methods and new opportunities, in *Tectonics of Sedimentary Basins: Recent Advance*, edited by C. Busby and A. Azor, pp. 47–62, Wiley-Blackwell, Oxford, U. K.
- Gehrels, G. E., et al. (2011), Detrital zircon geochronology of pre-tertiary strata in the Tibetan-Himalayan orogen, *Tectonics*, 30, TC5016, doi:10.1029/2011TC002868.
- Gerya, T. V., D. A. Yuen, and W. V. Maresch (2004), Thermomechanical modelling of slab detachment, *Earth Planet. Sci. Lett.*, 226(1), 101–116, doi:10.1016/j.epsl.2004.07.022.
- Gleadow, A. J. W., I. R. Duddy, P. F. Green, and J. F. Lovering (1986), Confined fission track lengths in apatite: A diagnostic tool for thermal history analysis, *Contrib. Mineral. Petrol.*, 94(4), 405–415.
- Godard, V., D. L. Bourlès, F. Spinabella, D. W. Burbank, B. Bookhagen, G. B. Fisher, A. Moulin, and L. Léanni (2014), Dominance of tectonics over climate in Himalayan denudation, *Geology*, 42(3), 243–246, doi:10.1130/G35342.1.
- Göğüş, O. H., and R. N. Pysklywec (2008), Mantle lithosphere delamination driving plateau uplift and synconvergent extension in eastern Anatolia, *Geology*, 36(9), 723–726, doi:10.1130/G24982A.1.
- Grujic, D., L. S. Hollister, and R. R. Parrish (2002), Himalayan metamorphic sequence as an orogenic channel: Insight from Bhutan, *Earth Planet. Sci. Lett.*, 198(1), 177–191, doi:10.1016/S0012-821X(02)00482-X.
- Guillot, S., A. Pêcher, P. Rochette, and P. LeFort (1993), The emplacement of the Manaslu granite of Central Nepal: Field and magnetic susceptibility constraints, in *Himalayan Tectonics*, edited by P. J. Treloar, and P. M. Searle, *Geol. Soc. London, Spec. Publ.*, 74, 413–428, doi:10.1144/GSL.SP.1993.074.01.28.
- Haider, V. L., I. Dunkl, H. von Eynatten, L. Ding, D. Frei, and L. Zhang (2013), Cretaceous to Cenozoic evolution of the northern Lhasa Terrane and the Early Paleogene development of peniplains at Nam Co, Tibetan Plateau, *J. Asian Earth Sci.*, 70–71, 79–98, doi:10.1016/j.jseas.2013.03.005.
- Herman, F., et al. (2010), Exhumation, crustal deformation, and thermal structure of the Nepal Himalaya derived from the inversion of thermochronological and thermobarometric data and modeling of the topography, *J. Geophys. Res.*, 115, B06407, doi:10.1029/2008JB006126.
- Hetzl, R., I. Dunkl, V. Haider, M. Strobl, H. von Eynatten, L. Ding, and D. Frei (2011), Peneplain formation in southern Tibet predates the India-Asia collision and plateau uplift, *Geology*, 39(10), 983–986, doi:10.1130/G32069.1.
- Hodges, K. V. (2000), Tectonics of the Himalaya and southern Tibet from two perspectives, *Geol. Soc. Am. Bull.*, 112(3), 324–350, doi:10.1130/0016-7606(2000)112<324:TOTHAS>2.0.CO;2.
- Hodges, K. V., R. R. Parrish, and M. P. Searle (1996), Tectonic evolution of the central Annapurna Range, Nepalese Himalayas, *Tectonics*, 15, 1264–1291, doi:10.1029/96TC01791.
- Huntington, K. W., A. E. Blythe, and K. V. Hodges (2006), Climate change and Late Pliocene acceleration of erosion in the Himalaya, *Earth Planet. Sci. Lett.*, 252(1), 107–118, doi:10.1016/j.epsl.2006.09.031.
- Husson, L., M. Bernet, S. Guillot, P. Huyghe, J. Mugnier, A. Replumaz, X. Robert, and P. van der Beek (2014), Dynamic ups and downs of the Himalaya, *Geology*, 42(10), 839–842, doi:10.1130/G36049.1.
- Jackson, S. E., N. J. Pearson, W. L. Griffin, and E. A. Belousova (2004), The application of laser ablation-inductively coupled plasma-mass spectrometry to un situ U-Pb zircon geochronology, *Chem. Geol.*, 211, 47–69, doi:10.1016/j.chemgeo.2004.06.017.
- Kali, E., P. H. Leloup, N. Arnaud, G. Mahéo, D. Liu, E. Boutonnet, J. Van der Woerd, X. Liu, J. Liu-Zeng, and H. Lin (2010), Exhumation history of the deepest central Himalayan rocks, Ama Drime range: Key pressure-temperature-deformation-time constrains on orogenic models, *Tectonics*, 29, TC2014, doi:10.1029/2009TC002551.
- Kapp, P., and J. H. Guynn (2004), Indian punch rifts Tibet, *Geology*, 32(11), 993–996, doi:10.1130/G20689.1.
- Kapp, P., P. G. Decelles, A. L. Leier, J. M. Fabijanic, S. He, A. Pullen, G. E. Gehrels, and L. Ding (2007), The Gangdese retroarc thrust belt revealed, *Geol. Soc. Am. Today*, 17(7), 4–9, doi:10.1130/GSAT01707A.1.
- Kawakami, T., M. Aoya, S. R. Wallis, J. Lee, K. Terada, Y. Wang, and M. Heizler (2007), Contact metamorphism in the Malashan dome, North Himalayan gneiss domes, southern Tibet: An example of shallow extensional tectonics in the Tethys Himalaya, *J. Metamorph. Geol.*, 25, 831–853, doi:10.1111/j.1525-1314.2007.00731.x.
- Kellett, D. A., D. Grujic, and S. Erdmann (2009), Miocene structural reorganization of the South Tibetan detachment, eastern Himalaya: Implications for continental collision, *Lithosphere*, 1(5), 259–281, doi:10.1120/L56.1.
- Kellett, D. A., and D. Grujic (2012), New insight into the South Tibetan detachment system: Not a single progressive deformation, *Tectonics*, 31, TC2007, doi:10.1029/2011TC002957.
- Kellett, D. A., D. Grujic, I. Coutand, J. Cottle, and M. Mukul (2013), The South Tibetan detachment system facilitates ultra rapid cooling of granulite-facies rocks in Sikkim Himalaya, *Tectonics*, 32, 252–270, doi:10.1002/tect.20014.
- Larson, K. P., L. Godin, W. J. Davis, and D. W. Davis (2010), Out-of-sequence deformation and expansion of the Himalayan orogenic wedge: Insight from the Changgo culmination, south central Tibet, *Tectonics*, 29, TC4013, doi:10.1029/2008TC002393.

- Law, R. D., M. P. Searle, and R. L. Simpson (2004), Strain, deformation temperatures and vorticity of flow at the top of the Greater Himalayan Slab, Everest Massif, Tibet, *J. Geol. Soc.*, *161*, 305–320, doi:10.1144/0016-764903-047.
- Le Fort, P. (1975), Himalayas: The collided range. Present knowledge of continental arc, *Amer. J. Sci.*, *275-A*, 1–44.
- Le Fort, P. (1996), Evolution of the Himalaya, in *The Tectonics of Asia*, edited by A. Yin and T. M. Harrison, pp. 95–106, Cambridge Univ. Press, New York.
- Lee, J., and M. J. Whitehouse (2007), Onset of mid-crustal extension flow in southern Tibet: Evidence from U/Pb zircon ages, *Geology*, *35*, 45–48, doi:10.1130/G22842A.1.
- Lee, J., B. R. Hacker, W. S. Dinklage, Y. Wang, P. Gans, A. Calvert, J. L. Wan, W. J. Chen, A. E. Blythe, and W. McClelland (2000), Evolution of the Kangmar Dome, southern Tibet: Structural, petrologic, and thermochronologic constraints, *Tectonics*, *19*, 872–895, doi:10.1029/1999TC001147.
- Lee, J., B. R. Hacker, and Y. Wang (2004), Evolution of north Himalayan gneiss domes: Structural and metamorphic studies in Mabja dome, southern Tibet, *J. Struct. Geol.*, *26*, 2297–2316, doi:10.1016/j.jsg.2004.02.013.
- Lee, J., C. Hager, S. R. Wallis, D. F. Stockli, M. J. Whitehouse, M. Aoya, and Y. Wang (2011), Middle to late Miocene extremely rapid exhumation and thermal reequilibration in the Kung Co rift, southern Tibet, *Tectonics*, *30*, TC2007, doi:10.1029/2010TC002745.
- Leloup, P. H., G. Mahéo, N. Arnaud, E. Kali, E. Boutonnet, D. Y. Liu, X. H. Liu, and H. B. Li (2010), The South Tibet detachment shear zone in the Dinggye area: Time constraints on extrusion models of the Himalayas, *Earth Planet. Sci. Lett.*, *292*(1–2), 1–16, doi:10.1016/j.epsl.2009.12.035.
- Leloup, P. H., X. H. Liu, G. Mahéo, J. Paquette, N. Arnaud, A. Aubray, and X. B. Liu (2015), New constrains on the timing of partial melting and deformation along the Nyalam section (central Himalaya): Implications for extrusion models, *Geol. Soc. London Spec. Publ.*, *412*, 131–175, doi:10.1144/SP412.11.
- Li, G., Y. Tian, B. P. Kohn, M. Sandiford, Z. Xu, and Z. Cai (2015), Cenozoic low temperature cooling history of the Northern Tethyan Himalaya in Zedang, SE Tibet and its implications, *Tectonophysics*, *643*, 80–93, doi:10.1016/j.tecto.2014.12.014.
- Li, M., A. Wang, C. Liu, G. Wang, and T. Li (2013), Neogene exhumation of the Greater Himalaya Slab in Gyirong area, Tibet, constrained by fission track geochronology, *Geol. Bull. China*, *32*, 86–92.
- Liu, G., and G. Einsele (1994), Sedimentary history of the Tethyan basin in the Tibetan Himalayas, *Geol. Rundsch.*, *82*(1), 32–61.
- Liu, Y. S., Z. C. Hu, S. Gao, D. Günther, J. Xu, C. G. Gao, and H. H. Chen (2008), In situ analysis of major and trace elements of anhydrous minerals by LA-ICP-MS without applying an internal standard, *Chem. Geol.*, *257*(1), 34–43, doi:10.1016/j.chemgeo.2008.08.004.
- Liu, Y. S., S. Gao, Z. C. Hu, C. G. Gao, K. Q. Zong, and D. B. Wang (2010), Continental and oceanic crust recycling-induced melt-peridotite interactions in the Trans-North China Orogen: U-Pb dating, Hf isotopes and trace elements in zircons of mantle xenoliths, *J. Petrol.*, *51*, 537–571, doi:10.1093/petrology/egp082.
- Ludwing, K. R. (2012), *User's Manual for Isoplot 3.75: A Geochronology Toolkit for Microsoft Excel*, Spec. Publ., vol. 5, pp. 1–75, Berkely Geochronol. Center, Berkeley, Calif.
- Mahéo, G., P. H. Leloup, F. Valli, R. Lacassin, N. Arnaud, J. Paquette, A. Fernandez, H. B. Li, K. Farley, and P. Tapponnier (2007), Post 4 Ma initiation of normal faulting in southern Tibet. Constraints from the Kung Co half graben, *Earth Planet. Sci. Lett.*, *256*, 233–243, doi:10.1016/j.epsl.2007.01.029.
- Molnar, P., and J. M. Stock (2009), Slowing of India's convergence with Eurasia since 20 Ma and its implications for Tibetan mantle dynamics, *Tectonics*, *28*, TC3001, doi:10.1029/2008TC002271.
- Mugnier, J. L., and P. Huyghe (2006), Ganges basin geometry records a pre-15 Ma isostatic rebound of Himalaya, *Geology*, *34*(6), 445–448, doi:10.1130/G22089.1.
- Murphy, M. A., and A. Yin (2003), Structural evolution and sequence of thrusting in the Tethyan fold-thrust belt and Indus-Yalu suture zone, southwest Tibet, *Geol. Soc. Am. Bull.*, *115*(1), 21–34, doi:10.1130/0016-7606(2003)115<0021:SEASOT>2.0.CO;2.
- Najman, Y. (2006), The detrital record of orogenesis: A review of approaches and techniques used in the Himalaya sedimentary basins, *Earth Sci. Rev.*, *74*, 1–72, doi:10.1016/j.earscirev.2005.04.004.
- Najman, Y., and E. Garzanti (2000), Reconstructing early Himalayan tectonic evolution and paleogeography from Tertiary foreland basin sedimentary rocks, northern India, *Geol. Soc. Am. Bull.*, *112*(3), 435–449, doi:10.1130/0016-7606(2000)112<435:REHTEA>2.0.CO;2.
- Najman, Y., et al. (2010), Timing of India-Asia collision: Geological, biostratigraphic, and palaeomagnetic constraints, *J. Geophys. Res.*, *115*, B12416, doi:10.1029/2010JB007673.
- Naylor, M., H. D. Sinclair, M. Bernet, P. A. van der Beek, and L. Kirstein (2015), Bias in detrital fission track grain-age populations: Implications for reconstructing changing erosion rates, *Earth Planet. Sci. Lett.*, *42*, 94–104, doi:10.1016/j.epsl.2015.04.020.
- Orme, D. A., P. W. Reiners, J. K. Hourigan, and B. Carrapa (2015), Effects of inherited cores and magmatic overgrowths on zircon (U-Th)/He ages and age-eU trends from Greater Himalayan sequence rocks, Mount Everest region, Tibet, *Geochem. Geophys. Geosyst.*, *16*, 2499–2507, doi:10.1002/2015GC005818.
- Quigley, M., Y. Liangjun, L. Xiaohan, C. J. L. Wilson, M. Sandiford, and D. Phillips (2006), <sup>40</sup>Ar/<sup>39</sup>Ar thermochronology of the Kampa Dome, southern Tibet: Implications for tectonic evolution of the North Himalayan gneiss domes, *Tectonophysics*, *421*(3), 269–297, doi:10.1016/j.tecto.2006.05.002.
- Ratschbacher, L., I. Krumrei, M. Blumenwitz, M. Staiger, R. Gloaguen, B. V. Miller, S. D. Samson, M. A. Edwards, and E. Appel (2011), Rifting and strike-slip shear in central Tibet and the geometry, age and kinematics of upper crustal extension in Tibet, *Geol. Soc. London Spec. Publ.*, *353*, 127–163, doi:10.1144/SP353.8.
- Replumaz, A., A. M. Negrodo, S. Guillot, and A. Villaseñore (2010), Multiple episodes of continental subduction during India/Asia convergence: Insight from seismic tomography and tectonic reconstruction, *Tectonophysics*, *483*, 125–134, doi:10.1016/j.tecto.2009.10.007.
- Robert, X., P. van der Beek, J. Braun, C. Perry, M. Dubille, and J. L. Mugnier (2009), Assessing Quaternary reactivation of the Main Central thrust zone (central Nepal Himalaya): New thermochronologic data and numerical modeling, *Geology*, *37*(8), 731–734, doi:10.1130/G25736A.1.
- Rohrmann, A., P. Kapp, B. Carrapa, P. W. Reiners, J. Guynn, L. Ding, and M. Heizler (2012), Thermochronologic evidence for plateau formation in central Tibet by 45 Ma, *Geology*, *40*(2), 187–190, doi:10.1130/G32530.1.
- Schlische, R. W. (1991), Half-graben basin filling models: New constraints on continental extensional basin development, *Basin Res.*, *3*(3), 123–141, doi:10.1111/j.1365-2117.1991.tb00123.x.
- Searle, M. P., R. R. Parrish, K. V. Hodges, A. Hurford, M. W. Ayres, and M. J. Whitehouse (1997), Shisha Pangma Leucogranite, South Tibetan Himalaya: Field relations, geochemistry, age, origin, and emplacement, *J. Geol.*, *105*(3), 295–318, doi:10.1086/515924.
- Stewart, R. J., and M. T. Brandon (2004), Detrital-zircon fission-track ages for the “Hoh Formation”: Implications for the late Cenozoic evolution of the Cascadia subduction wedge, *Geol. Soc. Am. Bull.*, *116*(1–2), 60–75, doi:10.1130/B22101.1.
- Sundell, K. E., M. H. Taylor, R. H. Styrón, D. F. Stockli, P. Kapp, C. Hager, D. Liu, and L. Ding (2013), Evidence for constriction and Pliocene acceleration of east-west extension in the North Lunggar rift region of west central Tibet, *Tectonics*, *32*, 1454–1479, doi:10.1002/tect.20086.

- Szulc, A., et al. (2006), Tectonic evolution of the Himalaya constrained by detrital  $^{40}\text{Ar}$ - $^{39}\text{Ar}$ , Sm-Nd and petrographic data from the Siwalik foreland basin succession, SW Nepal, *Basin Res.*, 18(4), 375–391, doi:10.1111/j.1365-2117.2006.00307.x.
- Tagami, T., and P. B. O'Sullivan (2005), Fundamentals of fission-track thermochronology, *Rev. Mineral. Geochem.*, 58(1), 19–47, doi:10.2138/rmg.2005.58.2.
- Thiede, R. C., and T. A. Ehlers (2013), Large spatial and temporal variations in Himalaya denudation, *Earth Planet. Sci. Lett.*, 371–372, 278–293, doi:10.1016/j.epsl.2013.03.004.
- Thiede, R. C., B. Bookhagen, J. R. Arrowsmith, E. R. Sobel, and M. R. Strecker (2004), Climatic control on rapid exhumation along the Southern Himalayan Front, *Earth Planet. Sci. Lett.*, 222, 791–806, doi:10.1016/j.epsl.2004.03.015.
- Tremblay, M. M., M. Fox, J. L. Schmidt, A. Tripathy-Lang, M. M. Wielicki, T. M. Harrison, P. K. Zeitler, and D. L. Shuster (2015), Erosion in southern Tibet shut down at ~10 Ma due to enhanced rock uplift within the Himalaya, *Proc. Nat. Acad. Sci.*, 112(39), 12,030–12,035, doi:10.1073/pnas.1515652112.
- van der Beek, P., X. Robert, J.-L. Mugnier, M. Bernet, P. Huyghe, and E. Labrin (2006), Late Miocene—Recent exhumation of the central Himalaya and recycling in the foreland basin assessed by apatite fission-track thermochronology of Siwalik sediments, Nepal, *Basin Res.*, 18, 413–434, doi:10.1111/j.1365-2117.2006.00305.x.
- Wang, A., J. I. Garver, G. Wang, J. A. Smith, and K. Zhang (2010), Episodic exhumation of the Greater Himalayan Sequence since the Miocene constrained by fission track thermochronology in Nyalam, central Himalaya, *Tectonophysics*, 495, 315–323, doi:10.1016/j.tecto.2010.09.037.
- Wang, F., S. Li, X. Shen, J. Zhang, and G. Yan (1996), Formation, evolution and environmental changes of the Gyirong basin and uplift of the Himalaya, *Sci. China Earth Sci.*, 39, 401–409.
- Wang, G., K. Cao, K. Zhang, A. Wang, C. Liu, Y. Meng, and Y. Xu (2011), Spatio-temporal framework of tectonic uplift stages of the Tibetan Plateau in Cenozoic, *Sci. China Earth Sci.*, 54(1), 29–44, doi:10.1007/s11430-010-4110-0.
- Wang, G., K. Cao, A. Wang, T. Shen, K. Zhang, and L. Wang (2014), On the geodynamic mechanism of episodic uplift of the Tibetan Plateau during the Cenozoic Era, *Acta Geol. Sin-Engl.*, 88(2), 699–716, doi:10.1111/1755-6724.12223.
- Wiesmayr, G. (2000), Eohimalaya structural evolution of the fold and thrust belt in the Tethyan Himalaya (Spiti, N-India), Ph.D. Thesis, Univ. of Wien, Vienna, Austria.
- Wiesmayr, G., and B. Grasemann (1999), Balanced cross-section and depth to detachment calculations for the Tethyan Himalaya (Spiti, N India): Where is the crystalline basement of the Higher Himalaya? *Terra Nostra*, 2, 172–173.
- Williams, H., C. Prince, T. Argles, and N. B. W. Harris (2001), Thermal evolution of the Himalayan metamorphic belt, Garhwal, India: Constraints from  $^{40}\text{Ar}$ - $^{39}\text{Ar}$  and Sm-Nd data, *J. Asian Earth Sci.*, 19, 75.
- Wu, C., K. D. Nelson, G. Wortmann, S. D. Samson, Y. Yue, J. Li, W. S. F. Kidd, and M. A. Edwards (1998), Yadong cross structure and South Tibetan detachment in the east central Himalaya (89°–90°E), *Tectonics*, 17, 28–45, doi:10.1029/97TC03386.
- Xu, Y., K. Zhang, G. Wang, S. Jiang, F. Chen, S. Xiang, G. Dupont-Nivet, and C. Hoorn (2012), Extended stratigraphy, palynology and depositional environments record the initiation of the Himalayan Gyirong Basin (Neogene China), *J. Asian Earth Sci.*, 44, 77–93, doi:10.1016/j.jseas.2011.04.007.
- Yang, X., J. Zhang, G. Qi, D. Wang, L. Guo, P. Li, and J. Liu (2009), Structure and deformation around the Gyirong basin, north Himalaya, and onset of the south Tibetan detachment system, *Sci. China Earth Sci.*, 52(8), 1046–1058, doi:10.1007/s11430-009-0111-2.
- Yin, A. (2006), Cenozoic tectonic evolution of the Himalayan orogen as constrained by along-strike variation of structural geometry, exhumation history, and foreland sedimentation, *Earth Sci. Rev.*, 79, 1–131, doi:10.1016/j.earscirev.2005.05.004.
- Yue, L. P., T. Deng, R. Zhang, Z. Q. Zhang, F. Heller, J. Q. Wang, and L. R. Yang (2004), Paleomagnetic chronology and records of Himalayan uplift on the Longgugou section of Gyirong-Oma Basin in Xizang (Tibet), *Chinese J. Geophys.*, 47(6), 1135–1142.
- Zhang, Z. (2002), *Geological map of the Gyirong County at a scale of 1:250,000 and geological report*, Hebei Inst. of Regional Geol. and Mineral Resour., Langfang, China.
- Zhisheng, A., J. E. Kutzbach, W. L. Prell, and S. C. Porter (2001), Evolution of Asian monsoons and phased uplift of the Himalaya-Tibetan Plateau since Late Miocene times, *Nature*, 411(6833), 62–66, doi:10.1038/35075035.